HOKKAIDO UNIVERSITY

Title	Skin permeability barrier formation by the ichthyosis-causative gene FATP4 through formation of the barrier lipid omega-O-acylceramide
Author(s)	Yamamoto, Haruka; Hattori, Miku; Chamulitrat, Walee; Ohno, Yusuke; Kihara, Akio
Citation	Proceedings of the National Academy of Sciences of the United States of America (PNAS), 117(6), 2914-2922 https://doi.org/10.1073/pnas.1917525117
Issue Date	2020-02-11
Doc URL	http://hdl.handle.net/2115/79050
Type	article (author version)
File Information	WoS_92677_Kihara.pdf

Instructions for use

Hokkaido University Collection of Scholarly and Academic Papers : HUSCAP

Skin permeability barrier formation by the ichthyosis-causative gene *FATP4* through formation of the barrier lipid ω-*O*-acylceramide

Haruka Yamamoto[a,1], Miku Hattori[a,1], Walee Chamulitrat[b], Yusuke Ohno[a], and Akio Kihara[a,2]

[a]Laboratory of Biochemistry, Faculty of Pharmaceutical Sciences, Hokkaido University, Kita 12-jo, Nishi 6-chome, Kita-ku, Sapporo 060-0812, Japan.

[b]Department of Internal Medicine IV, Heidelberg University Hospital, Im Neuenheimer Feld 410, 69120 Heidelberg, Germany.

[1]H.Y. and M.H. contributed equally to this work.

[2]To whom correspondence may be addressed.

Akio Kihara

Laboratory of Biochemistry, Faculty of Pharmaceutical Sciences

Hokkaido University

Kita 12-jo, Nishi 6-chome, Kita-ku, Sapporo 060-0812, Japan

Tel: +81-11-706-3754

Fax: +81-11-706-4900

E-mail: kihara@pharm.hokudai.ac.jp

Author ORCIDs

Yusuke Ohno ID: https://orcid.org/0000-0003-3702-1043

Akio Kihara ID: https://orcid.org/0000-0001-5889-0788

Abstract

The epidermis-specific lipid acylceramide plays a pivotal role in the formation of the permeability barrier in the skin; abrogation of its synthesis causes the skin disorder ichthyosis. However, the acylceramide synthetic pathway has not yet been fully elucidated: namely, the acyl-CoA synthetase (ACS) involved in this pathway remains to be identified. Here, we hypothesized it to be encoded by *FATP4*/*ACSVL4*, the causative gene of ichthyosis prematurity syndrome (IPS). *In vitro* experiments revealed that FATP4 exhibits ACS activity toward an ω-hydroxy fatty acid (FA), an intermediate of the acylceramide synthetic pathway. *Fatp4* knockout (KO) mice exhibited severe skin barrier dysfunction and morphological abnormalities in the epidermis. The total amount of acylceramide in *Fatp4* KO mice was reduced to ~10% of wild type mice. Decreased levels and shortening of chain-lengths were observed in the saturated, non-acylated ceramides. FA levels were not decreased in the epidermis of *Fatp4* KO mice. The expression levels of the FA elongase *Elovl1* were reduced in *Fatp4* KO epidermis, partly accounting for the reduction and shortening of saturated, non-acylated ceramides. A decrease in acylceramide levels was also observed in human keratinocytes with *FATP4* knockdown. From these results, we conclude that skin barrier dysfunction observed in IPS patients and *Fatp4* KO mice is caused mainly by reduced acylceramide production. Our findings further elucidate the molecular mechanism governing acylceramide synthesis and the IPS pathology.

Keywords: acylceramide; ceramide; lipid; skin; sphingolipid.

Significance statement

Acylceramide is essential for skin permeability barrier formation. However, its biosynthesis pathway has not yet been elucidated in its entirety. In the present study, we found that *Fatp4* disruption substantially decreased the amount of acylceramides in mice, as did *FATP4* knockdown in human keratinocytes. In addition, *in vitro* experiments demonstrated that FATP4 exhibited acyl-CoA synthetase activity toward an ω-hydroxy ultra-long-chain fatty acid, an intermediate of the acylceramide biosynthetic pathway. From these results, we conclude that FATP4 functions in skin barrier formation through acylceramide synthesis. Our findings not only reveal the pathogenic mechanism of ichthyosis prematurity syndrome, but also help to elucidate the molecular mechanism of the synthesis of the skin barrier lipid acylceramide.

Introduction

Skin possesses a powerful permeability barrier (the skin barrier), which functions to prevent infectious diseases and allergies by blocking the invasion of external substances such as pathogens, allergens, and chemicals. It also prevents water loss from the body, an essential function for terrestrial animals. The skin barrier is so strong that infections through the skin rarely occur under normal circumstances; but if it is damaged, such as by a burn or cut, the risk of infection increases dramatically. Ichthyosis is an inherited disease featuring skin barrier abnormalities and is characterized by dryness, thickening, and scaly skin (1). Similarly, atopic dermatitis patients suffer from reduced skin barrier function, allowing allergens to enter (2).

Ichthyosis prematurity syndrome (IPS) is one of the syndromic forms of ichthyosis (3, 4). IPS is characterized by premature birth, neonatal asphyxia, and ichthyosis. Ichthyosis improves during the first several weeks after birth but persist for life, often accompanying atopic dermatitis and recurrent infections. The epidermis of IPS patients is thickened, and hyperkeratosis and presence of droplets are observed in the stratum corneum (3, 5). Furthermore, curved multilamellar membranes exist in the stratum corneum and granular layer of such patients (3, 5, 6). The causative gene of IPS is *FATP4* [fatty acid transporter, member 4; also known as *ACSVL4* (acyl-CoA synthetase very-long-chain, member 4) or *SLC27A4* (solute carrier family 27, member 4)] (3). As the alternative name of FATP4, ACSVL4, indicates, FATP4 is an acyl-CoA synthetase (ACS) that converts fatty acids (FAs) to acyl-CoAs. FAs are classified by chain length; long-chain (LC) FAs have a chain length of C11–C20 and very-long-chain (VLC) FAs have a length of ≥C21. VLCFAs with ≥C26 are sometimes denominated ultra-long-chain (ULC) FAs, since their functions and tissue distributions differ from shorter VLCFAs (7, 8). FATP4/ACSVL4 belongs to the very-long (VL) subfamily of ACSs and exhibits higher ACS activity toward VLCFAs than LCFAs (9).

Several *Fatp4* knockout (KO) mice have been reported, either generated spontaneously or by gene targeting (10-14). Except for one report indicating prenatal lethality (12), *Fatp4* KO mice are neonatal lethal (10, 11, 13, 14). Newborn *Fatp4* KO mice exhibit severe skin barrier abnormalities, hyperkeratosis, keratinocyte hyperproliferation, acanthosis, and small keratohyalin granules (10, 11, 13, 14). In addition, the rigid skin of *Fatp4* KO mice causes facial dysmorphia, movement restriction, and respiratory failure. However, the mechanism by which mutations in the *FATP4*/*Fatp4* gene cause ichthyosis in IPS patients and *Fatp4* KO mice remains unclear.

Lipids are suitable for the formation of permeability barriers due to their high hydrophobicity. The stratum corneum contains a multilayer lipid structure (the lipid lamellae) that plays a central role in skin barrier formation (8, 15). The lipid lamellae are mainly composed of ceramides, FAs, and cholesterol. Ceramide forms the backbone of sphingolipids (biological membrane lipids) consisting of two hydrophobic chains: a long-chain base and an FA (Fig. 1*A*). In addition to this normal-type ceramide, acylceramide (ω-*O*-acylceramide), a ceramide class specialized for skin barrier formation, exists in the epidermis (8, 16, 17). Acylceramide shows a unique three hydrophobic-chain structure, in which linoleic acid is esterified to the ω-position of the FA moiety of ceramide (Fig. 1*B*). As a C30–36 ULCFA, acylceramide also has a characteristic and much longer FA chain length than normal ceramide (C16–24). The unique structure of acylceramide is important for the formation and maintenance of lipid lamellae, and skin barrier formation: mutations in the human genes involved in its synthesis cause autosomal recessive congenital ichthyosis, the most severe type in the family of disorders (1, 8, 17, 18). In mice, these mutations lead to neonatal lethality due to skin barrier dysfunction (19-24).

Despite the importance of acylceramide in skin barrier formation, most of the genes involved in acylceramide production have only recently been identified. The identified genes include the FA elongases *ELOVL1* and *ELOVL4* for elongation of FAs up to C30–C36 (19, 21, 25), the ceramide synthetase *CERS3* for amide bond formation between a long-chain base and a ULCFA (20), the cytochrome P450 member *CYP4F22* for ULCFA ω-hydroxylation (26), and the transacylase *PNPLA1* for ester bond formation between a ULCFA and a linoleic acid (22-24, 27) (*SI Appendix*, Fig. S1).

We previously identified the above-mentioned FA ω-hydroxylase gene *CYP4F22*, which hydroxylates the ω-position of ULCFAs (26). *CYP4F22* is one of the causative genes of autosomal recessive congenital ichthyosis (28-30), and the amount of acylceramide was greatly reduced in the patient examined in that study (26). We also found that the substrates of CYP4F22 are ULCFAs using biochemical and cell-based assays (26). The FA elongases ELOVL1 and ELOVL4 are responsible for the elongation of shorter FAs to ULCFAs (19, 21, 25). Since the elongation reactions proceed in acyl-CoA forms (7, 8), ULC acyl-CoAs produced by the FA elongases must be converted to ULCFAs in order to be catalyzed by CYP4F22. After ω-hydroxylation by CYP4F22, the resulting ω-hydroxy (ω-OH) ULCFAs need to be re-converted to acyl-CoA forms, the substrates of the subsequent reaction catalyzed by the ceramide synthase CERS3 (20). However, the ACS involved in this reaction has remained unknown.

Given the importance of acylceramide in skin barrier formation, mutations in the unidentified *ACS* gene in the acylceramide synthesis pathway are expected to cause congenital ichthyosis. Twenty-six *ACSs* exist in mammals (31). Of these, we speculate that *FATP4* is the unidentified *ACS* gene that functions in the acylceramide synthesis pathway, based on the severe skin symptoms/phenotypes observed in human IPS patients and *Fatp4* KO mice. Since

no hypotheses about the involvement of *FATP4* in acylceramide synthesis have been proposed so far, acylceramide levels have not yet been measured in *Fatp4* KO mice. Shortening of the chain length of non-acylated (normal-type) ceramides has been reported in *Fatp4* KO mice: specifically, decreases in ≥C26 ceramides and increases in ≤C24 ceramides (10). In the present study, we performed several analyses of *Fatp4* KO mouse epidermis to examine the function of *Fatp4* in acylceramide synthesis and to reveal the causes of skin barrier dysfunction observed in IPS patients.

Results

Abnormalities in Skin Barrier Formation and Epidermal Morphology in *Fatp4* KO Mice. To date, several *Fatp4* mutant mouse lines have been generated (10-14). To investigate the involvement of *FATP4* in acylceramide synthesis in the present study, we created another *Fatp4* KO mouse line by genome editing using CRISPR/Cas9. Setting the target sequence to exon 3 of the *Fatp4* gene, we obtained *Fatp4* KO mice having a single nucleotide insertion between the 196th thymine and the 197th guanine in the coding sequence (Fig. 1*C*). This gene product is predicted to contain the N-terminal 66 amino acids of wild type (WT) protein (643 amino acids) followed by an unrelated 42 amino acids, due to a frameshift and its accompanying early stop codon. Since the translated region is very short, this mutated gene product is expected to be completely non-functional. As in the previously reported *Fatp4* mutant mice (10, 11, 14), our *Fatp4* KO mice also had more rigid, less wrinkled skin than WT mice (Fig. 1*D*) and were neonatal lethal. We then examined the time course of the survival rates of the mice obtained by cesarean section on embryonic day 18.5 (E18.5). All KO mice died within 1 h after cesarean section (Fig. 1*E*). Under the same conditions, where newborn mice were taken from their mothers and could not drink milk, even WT mice did not survive beyond 22 h after cesarean section. The body weight of E18.5 KO mice was lower than that of WT mice (Fig. 1*F*). The value of the transepidermal water loss (TEWL), an index of the skin permeability barrier function from inside the body to the outside, was 4.4-fold higher in *Fatp4* KO mice than WT mice (Fig. 1*G*). The inverse skin permeability barrier function, from the outside to the body, was examined by toluidine blue staining. Little dye penetration was observed in WT mice, while strong penetration was observed in *Fatp4* KO mice (Fig. 1*H*). These high TEWL values and enhanced dye staining have also been reported in the previous

Fatp4 KO mice (10, 13), confirming the presence of impaired skin barrier function in our newly created *Fatp4* KO mice.

Hematoxylin/eosin staining was conducted to examine morphological changes in the epidermis of *Fatp4* KO mice. In the stratum corneum of WT mice, inter-corneocyte gaps, which correspond to lipid lamellae, were observed (Fig. 2*A*). In *Fatp4* KO mice, the existence of gaps was less obvious, indicating impaired lipid lamellae formation. Acanthosis was observed in the stratum spinosum of *Fatp4* KO mice. A more detailed examination of the structure of the epidermis was carried out by transmission electron microscopy. The number of cell layers in the stratum corneum was increased in *Fatp4* KO mice compared to WT mice (Fig. 2*B* and *C*). The existence of keratohyalin granules filled with profilaggrin is a feature of the stratum granulosum. These granules in *Fatp4* KO mice were smaller than those in WT mice (Fig. 2*B*). Hyperkeratosis, acanthosis, and small keratohyalin granules were also observed in the previously reported *Fatp4* mutant mice (10, 11, 13, 14). We found vacuoles and curved membrane structures, which may represent deposits of lipids/membranes probably caused by impaired lamellar body release, in the stratum corneum of *Fatp4* KO mice (Fig. 2*C* and *D*). Similar structures have also been observed in IPS patients (3, 5, 6). These morphological abnormalities suggest that keratinocyte differentiation and lipid lamellae formation are impaired in the *Fatp4* KO mouse epidermis.

Decreased Amount of Acylceramide in *Fatp4* KO Mouse Epidermis. To examine the effect of *Fatp4* disruption on epidermal lipid composition, lipids were extracted from the mouse epidermis, separated by thin layer chromatography (TLC), and stained with copper sulfate/phosphoric acid solution. We observed decreases in the amounts of acylceramide and acyl-glucosylceramide in *Fatp4* KO mice compared with WT mice, whereas FA and

triglyceride (TAG) levels were increased (Fig. 3*A*). No apparent differences between WT and *Fatp4* KO mice were found in the amounts of cholesterol and glycerophospholipids.

Quantitative analysis of acylceramide species was performed using liquid chromatography (LC) coupled with tandem mass spectrometry (MS/MS). In *Fatp4* KO mice, the amounts of all of the acylceramide species, regardless of FA chain length and degree of unsaturation (saturated or monounsaturated), were substantially decreased compared with those in WT mice (Fig. 3*B* and *C*). The total amount of acylceramides in *Fatp4* KO mice was 9.8 % of WT mice, with saturated and monounsaturated acylceramides being similarly reduced (saturated, 7.4 %; monounsaturated, 11 %). These results indicate that Fatp4 is indeed involved in the acylceramide synthesis.

We also measured the amounts of acyl-glucosylceramides, which are acylceramide metabolites (*SI Appendix*, Fig. S1). The total amount of saturated acyl-glucosylceramides was substantially reduced in *Fatp4* KO mice (9.1 % of WT mice; Fig. 3*D*), as was that of saturated acylceramides (Fig. 3*C*). On the other hand, the decrease in the total amount of monounsaturated acyl-glucosylceramides in KO mice was rather small (46 % of WT mice; Fig. 3*D*), in contrast to that of monounsaturated acylceramides (Fig. 3*C*). The total amount of acyl-glucosylceramides (saturated plus monounsaturated) was 37 % of that in WT mice (Fig. 3*D*).

We next measured the amounts of protein-bound ceramides in *Fatp4* KO mice, into which a portion of the acylceramide is converted (*SI Appendix*, Fig. S1). Protein-bound ceramide is a crucial component of a unique membrane structure to corneocytes, termed the corneocyte lipid envelope, which is thought to function in connecting lipid lamellae and corneocytes (32-34). Again, a difference in the degree of reduction between saturated and monounsaturated types owing to *Fatp4* disruption was observed. The amount of total saturated protein-bound ceramides in *Fatp4* KO mice was reduced to 6.8 % of that in WT mice, whereas the total

amount of monounsaturated protein-bound ceramides remained comparable (Fig. 3*E*). In addition, the total amount of protein-bound ceramides (saturated plus monounsaturated) was 65 % of that in WT mice.

The final step of acylceramide production is the ester bond formation between ω-OH ceramide and linoleic acid (*SI Appendix*, Fig. S1). This reaction is catalyzed by the transacylase PNPLA1, where PNPLA1 transfers the linoleic acid in TAG to ω-OH ceramide (27). We measured the amounts of ω-OH ceramides, which are precursors of acylceramides, and found a large decrease (64 % of WT mice) in the total amount of saturated ω-OH ceramides in *Fatp4* KO mice (Fig. 3*F*). In contrast, no difference was observed in the total amounts of monounsaturated ω-OH ceramides. The total amount of ω-OH ceramides (saturated plus monounsaturated) in *Fatp4* KO mice was decreased to 64 % of that in WT mice.

In the acylceramide synthetic pathway, ω-OH acyl-CoA, the product of FATP4, is converted to ω-OH ceramide, acylceramide, acyl-glucosylceramide, and protein-bound ceramide (Fig. 3*G* and *SI Appendix*, Fig. S1). The sum of all these ω-OH acyl-CoA metabolites in *Fatp4* KO mice was reduced to 25.6 % of WT mice (Fig. 3*H*). The decrease was large in saturated types (7.2 %) but smaller in monounsaturated types (33.5 %).

***Fatp4* Gene Disruption Does not Reduce the Uptake of FAs into the Epidermis.** Previous studies measuring ceramides (non-acylated, normal type) reported that ≥C26 ceramides were decreased in *Fatp4* KO epidermis compared with WT mice, whereas ≤C24 ceramides were increased (10). In the present study, we performed more detailed analyses. First, we confirmed the decreases in ≥C26 and increases in ≤C24 for saturated ceramides in the epidermis of the *Fatp4* KO mice (Fig. 4*A*), consistent with the previous report (10). While that study measured only C18:1 and C24:1 ceramides for monounsaturated ceramides (10), we here expanded the

analyses to ≥C24 monounsaturated species. As in the case of saturated ceramides, the amount of monounsaturated ceramide with a chain length of C24 was also increased in *Fatp4* KO mice compared with WT mice (Fig. 4*A*). On the other hand, unlike the saturated types, the amount of C26 monounsaturated ceramide was unchanged, and those of ≥C28 monounsaturated ceramides were unexpectedly increased. In summary, the total amount of ≤C24 ceramides was increased ~3-fold in *Fatp4* KO mice compared with WT mice, whereas that of ≥C26 saturated ceramides was decreased to 34 %. The total amount of ≥C26 monounsaturated ceramides as well as total amount of ceramides (saturated plus monounsaturated) was almost unchanged. Thus, *Fatp4* disruption had a greater effect on acylceramides than non-acylated ceramides. Similar changes in ceramide composition (increases in ≤C24 and decreases in ≥C26 ceramides; and large effects on saturated ceramides but mild effects on monounsaturated ceramides) were also observed in *Elovl1* (a FA elongase)-KO mice (21), implying a reduced activity of Elovl1 in *Fatp4* KO mice.

Since the effect of *Fatp4* disruption on the abundance of individual FA species has so far not been investigated using MS, we estimated species composition and abundance using epidermal samples. Similar to ceramides (Fig. 4*A*), the amounts of most ≤C24 FAs were increased in *Fatp4* KO mice compared with WT mice (Fig. 4*B*). In contrast, the amounts of ≥C26 saturated FAs in *Fatp4* KO mice were not significantly different from those in WT mice, and ≥C26 monounsaturated FAs were unexpectedly increased. The total amount of FAs in *Fatp4* KO mice was 2.1-fold higher than that of WT mice. The substrates of FA elongases in the FA elongation process are acyl-CoAs rather than FAs (7). Therefore, the VLCFAs and ULCFAs in *Fatp4* KO mice are most likely produced from the corresponding acyl-CoAs via hydrolysis of CoA by thioesterases after FA elongation. The increases in many FAs, especially monounsaturated FAs, in *Fatp4* KO mice suggest that FATP4 has a function of converting the

FAs generated by thioesterase back to acyl-CoAs. It is likely that the equilibrium between FAs and acyl-CoA shifts to FAs due to *Fatp4* disruption. Although an FA transporter function of FATP4 has been hypothesized (4, 11), our results (specifically the increases in the amounts of FAs in *Fatp4* KO mice) did not support this hypothesis. Since linoleic acid (C18:2), a component of acylceramide, is an essential FA that cannot be synthesized in mammals, keratinocytes must procure it from outside the cells. However, the amount of linoleic acid was also increased in *Fatp4* KO epidermis (Fig. 4*B*).

The linoleic acid moiety in acylceramide is derived from TAG; Pnpla1 transfers linoleic acid in TAG to ω-OH ceramide by transacylation (27) (*SI Appendix*, Fig. S1). We examined the amounts of linoleic acid-containing TAGs in the epidermis of *Fatp4* KO mice, and found that all TAG species examined were increased compared with WT mice (Fig. 4*C*). These results indicate that the skin barrier dysfunction and the decreased acylceramide in *Fatp4* KO mice are not due to reduced uptake of linoleic acid.

Decreased Expression of *Elovl1* and *Pnpla1* Due to *Fatp4* Disruption. Abnormalities in epidermal morphology and changes in lipid metabolism were observed in *Fatp4* KO mice (Figs. 2–4). To investigate the causes behind these changes, the expression levels of keratinocyte differentiation markers and lipid metabolism genes were analyzed by quantitative RT-PCR. Among keratinocyte differentiation markers, the stratum basale marker *Krt14* (keratin 14) showed a tendency to increase in *Fatp4* KO mice compared with WT mice, although this was not statistically significant (Fig. 5*A*). In contrast, *Krt10* (keratin 10), a marker of the stratum spinosum and stratum granulosum, was reduced in the KO mice (8.3 % of WT mice). The stratum granulosum markers *Flg* (filaggrin) and *Ivl* (involucrin) were also decreased (1.2 % and 7.8 % of WT mice, respectively). We confirmed decreases in the protein levels of filaggrin

and keratin 10 by immunoblotting (*SI Appendix*, Fig. S2). These results indicate that differentiation into stratum spinosum and/or stratum granulosum was impaired in the *Fatp4* KO mouse epidermis. Abnormal expression of differentiation markers has been observed in mice with KO of several genes involved in acylceramide synthesis (*Pnpla1*, *Cers3*, and *Cyp4f39* KO mice) (20, 22, 23, 35). Although the exact reason is unknown, it is possible that keratinocytes sense and respond to impaired lamellar body and lipid lamella formation.

Next, the expression levels of acylceramide synthesis-related genes were examined (Fig. 5*B*). The expression levels of the transacylase *Pnpla1* were reduced in the *Fatp4* KO mouse epidermis (32 % of WT mice), while almost no changes were observed in the expression levels of the ceramide synthetase *Cers3*, the FA ω-hydroxylase *Cyp4f39* (a mouse orthologue of human *CYP4F22*), or *Abhd5*, a gene product that functions to promote utilization of TAGs by Pnpla1 (36).

Since changes in the chain lengths of ceramides and FAs were observed (Fig. 4*A* and *B*), the expression levels of the FA elongase *Elovl* family members were examined. In *Fatp4* KO mice, the expression levels of *Elovl1* were reduced to 25 % of WT mice (Fig. 5*C*). *Elovl1* plays an important role in the elongation of C24:0-CoA to C26:0-CoA in epidermis (21). The expression levels of *Elovl4*, which is responsible for elongation of C26-CoA to ≥C28-CoAs (7, 8, 19), were reduced to 59 % of WT mice. The expression levels of *Elovl6* and *Elovl7*, which respectively exhibit activity towards C16:0-CoA and C18-CoAs (7, 8, 25), were reduced to about half the levels of WT mice.

We investigated the possibility of compensatory changes in the expression of other *Fatp*/*Acsvl* family members due to *Fatp4* disruption. In WT mice, expression levels of *Fatp4* were the highest among *Fatp* family members, as also observed in human keratinocytes (37). The expression levels of *Fatp4* were substantially reduced in *Fatp4* KO mice (Fig. 5*D*),

possibly due to destabilization of *Fatp4* mRNA by nonsense-mediated mRNA decay. In *Fatp4* KO mice, the expression levels of *Fatp1*, *Fatp2*, *Fatp3*, *Fatp5*, and *Fatp6* showed tendencies to increase, although these were not statistically significant. In summary, our results suggest that changes in ceramide/fatty acid chain lengths and decreased acylceramide levels observed in *Fatp4* KO mice are at least partly attributable to decreased expression levels of *Elovl1* and *Pnpla1*.

FATP4 Exhibits ACS Activity Toward ω-OH ULCFA. We speculate that FATP4 acts as an ACS that converts ω-OH ULCFAs to ω-OH ULC acyl-CoAs in the acylceramide synthetic pathway. However, it has not been examined whether FATP4 has ACS activity toward ω-OH ULCFAs, although activity toward LC and VLC non-hydroxylated FAs has been reported (9, 38, 39). Therefore, we performed *in vitro* ACS assays using ω-OH C30 FA as a substrate and membrane fractions prepared from HEK 293T cells overexpressing human FATP4 as enzyme source. Overexpression of FATP4 caused a 10.5-fold increase in ACS activity compared with control (Fig. 6). Furthermore, overexpression of FATP4 increased ACS activities toward C24:0 and C24:1 FAs by 6.6- and 3.5-fold, respectively. It is worthwhile to note that substrate preference for FATP4 among FA substrates cannot be evaluated by this method, since the water solubility of the substrate FAs, which affects the enzyme activity, and the ionization efficiency of the product acyl-CoAs are different. Our results indicate that FATP4 can indeed produce ω-OH ULC acyl-CoAs, which are required for acylceramide synthesis. In addition, our findings reveal that FATP4 is active toward a wide range of FAs from LC to ULC, regardless of non-hydroxylated or ω-hydroxylated status.

***FATP4* Knockdown in Human Keratinocytes Decreases Acylceramide Production.** We next performed knockdown analyses to investigate whether FATP4 is involved in acylceramide production in human keratinocytes. Human keratinocytes were infected with lentiviral plasmids to express an shRNA targeting *FATP4*, and they then differentiated. Two shRNAs targeting different *FATP4* sequences (sh*FATP4*-1 and sh*FATP4*-2) both showed a knockdown efficiency of over 90% (Fig. 7*A*). These *FATP4* shRNAs reduced the amounts of all C30-C36 acylceramide species, and they were decreased overall by ~40% compared to the control (Fig. 7*B* and *C*). On the other hand, the shRNAs did not affect the amounts of non-acylated ceramides (Fig. 7*D*). These results indicate that FATP4 is also involved in acylceramide production in human keratinocytes.

Discussion

Acylceramide is a lipid that is essential for skin barrier formation, and the abrogation of its production causes ichthyosis in humans and neonatal lethal barrier defects in mice (1, 8, 17-24). However, not all genes involved in the production of acylceramide have been identified to date. Based on our previous finding that the substrates of the FA ω-hydroxylase CYP4F22 are ULCFAs (26), we speculate that the acylceramide synthesis pathway includes three successive reactions: ULC acyl-CoA to ULCFAs by a thioesterase, ULCFAs to ω-OH ULCFAs by the FA ω-hydroxylase CYP4F22, and ω-OH ULCFAs to ω-OH ULC acyl-CoA by an ACS (*SI Appendix*, Fig. S1). Of these, the thioesterase and ACS remained to be identified. In the present study, we found that acylceramide levels in *Fatp4* KO mice are reduced to ~10 % of those in WT mice. Given this large decrease in acylceramide levels, it is reasonable to conclude that Fatp4 is directly involved in acylceramide production. We also confirmed the involvement of FATP4 in acylceramide production using human keratinocytes and knockdown analyses (Fig. 7). Furthermore, these results support the validity of our model, which assumes that ACS is involved in the acylceramide synthesis pathway. While the thioesterase(s) has not yet been identified, members of the ACOT (acyl-CoA thioesterase) family are considered candidates. Mammals have 15 ACOTs (ACOT1–13, THEM4, and THEM5), and it is possible that some of these redundantly function in acylceramide synthesis.

Several previous studies have generated *Fatp4* mutant mice and reported the presence of severe skin barrier abnormalities (10, 11, 13, 14). However, the mechanism that causes the abnormalities has remained unknown. One hypothesis as to the cause of the skin barrier dysfunction is the loss of FA transporter activity by Fatp4 (4, 11); another is changes in (non-acylated) ceramide metabolism (10). In recent years, many acylceramide-related genes have been identified, and the respective KO mice were created and analyzed. These mice exhibited

severe skin barrier abnormalities that resemble those observed in *Fatp4* mutant mice (19-24). This phenotypic resemblance led to our hypothesis that the impaired skin barrier formation observed in IPS patients and *Fatp4* mutant mice is caused by a defect in acylceramide synthesis. In the present study, we provided proof for this notion (Fig. 3*C*). With respect to the reduced FA uptake hypothesis, we found that the amounts of linoleic acid and linoleic acid-containing TAGs were not decreased but rather increased in the epidermis of *Fatp4* KO mice (Fig. 4*B* and *C*), contradicting the hypothesis. With respect to changes in (non-acylated) ceramide metabolism, the decreases in ≥C26 ceramides and increases in ≤C24 ceramides(10) (Fig. 4*A*) in *Fatp4* KO mice likely partly contribute to the skin barrier dysfunction. However, the effect of *Fatp4* disruption on the amounts of acylceramide was much greater than on ceramides. Furthermore, considering the severe skin barrier abnormality in *Pnpla1* KO mice in which only the amounts of acylceramides (but not of ceramides) are decreased (23, 24), it is very possible that the decreases in acylceramide amounts are mainly responsible for the observed skin barrier dysfunction.

The FA elongase Elovl1 plays important roles in the elongation of saturated VLC acyl-CoA, especially of C24:0-CoA to C26:0-CoA, although its contribution to the elongation of monounsaturated VLC acyl-CoAs is lower (21, 40). Expression levels of *Elovl1* were decreased in *Fatp4* KO mouse epidermis (Fig. 5*C*). Therefore, we speculate that this decrease in *Elovl1* expression causes the changes in ceramide metabolism—i.e., the decreases in ≥C26 saturated ceramides and increases in ≤C24 saturated ceramides—as observed in the epidermis of *Elovl1* KO mice (21). The exact cause for the decreased *Elovl1* expression is unknown. However, it is likely that impaired skin barrier formation due to reduced acylceramide production indirectly leads to expressional changes in various genes including *Elovl1* (*SI*

Appendix, Fig. S3*A*). Decreased expression of *Elovl1* has also been observed in KO mice of *Nipal4* (another ichthyosis-causative gene) (41).

The expression levels of *Pnpla1* were also reduced in *Fatp4* KO mice (Fig. 5*B*). Pnpla1 catalyzes the final step of acylceramide production, the conversion of ω-OH ceramide to acylceramide (27). The decreased expression of *Pnpla1* in *Fatp4* KO mice may be partly responsible for reduced acylceramide production. The monounsaturated ω-OH ceramide was unexpectedly not reduced in *Fatp4* KO mice (Fig. 3*F*). We speculate that two effects –reduced production due to *Fatp4* deficiency and substrate accumulation due to decreased expression of *Pnpla1* – acted in a mutually countervailing manner here.

The reaction products of Fatp4, ω-OH ULC acyl-CoAs, are rapidly metabolized to ω-OH ceramides, acylceramides, acyl-glucosylceramides, and protein-bound ceramides (Fig. 3*G* and *SI Appendix*, Fig. S1). Since ω-OH ULC acyl-CoAs are transient metabolic intermediates, the sum of the ω-OH ULC acyl-CoA metabolites, rather than the amounts of ω-OH ULC acyl-CoAs themselves, may represent the actual amounts of ω-OH ULC acyl-CoAs produced by Fatp4 (and other Fatp/Acsvl subfamily members having redundant functions). The sum of saturated ω-OH ULC acyl-CoA metabolites was reduced to ~1/14 by *Fatp4* disruption (Fig. 3*H*). We consider this to be caused by the combined effects of the decrease in the conversion step of ω-OH ULCFAs to ω-OH ULC acyl-CoAs due to *Fatp4* disruption, and the decreased supply of ULC acyl-CoAs due to reduced expression levels of *Elovl1* (*SI Appendix*, Fig. S3*B*). However, it is difficult to estimate the degree of contribution of the *Fatp4* disruption. On the other hand, since the contribution of Elovl1 to the elongation of the monounsaturated VLCFAs is small, the decrease in the sum of monounsaturated ω-OH ULC acyl-CoA metabolites as well as total amount of monounsaturated acylceramides can be considered to be simply due to *Fatp4* disruption (*SI Appendix,* Fig. S3*B*). Indeed, the amounts of non-acylated ceramides with

≥C30:1 were not reduced in *Fatp4* KO mice compared with WT mice (Fig. 4*A*), indicating that the amounts of ≥C30:1 acyl-CoAs were not reduced by the *Fatp4* disruption. In *Fatp4* KO mice, the sum of monounsaturated ω-OH ULC acyl-CoA metabolites was reduced to ~1/3 compared with WT mice (Fig. 3*H*). This implies that the contribution of Fatp4 to conversion of ω-OH ULCFAs to ω-OH ULC acyl-CoAs in the acylceramide production pathway is approximately ~2/3 of the total. This may even be an underestimate, considering that the expressions of other *Fatp* subfamily members had tendencies to increase in *Fatp4* KO mice (Fig. 5*D*). Among Fatp subfamily members, Fatp1 shares the highest amino acid sequence similarity with Fatp4, and forced expression of *Fatp1* in the epidermis of *Fatp4* KO mice can complement the skin barrier abnormalities (42).

In the present study, we elucidated one of the missing links in the acylceramide synthetic pathway. Furthermore, we revealed that the cause of IPS pathology is impaired acylceramide production, not reduction in FA uptake as assumed to date. Further research into the treatment of IPS with acylceramide or compounds with similar effects is thus required.

Methods

Extended details for all methods are available in *SI Appendix, Materials and Methods*.

Production and Breeding of Mice. *Fatp4* KO mice were generated by CRISPR/Cas9. Mice were housed at 23 ± 1°C ambient temperature and at 50 ± 5% humidity with a 12 h light/dark cycle with food available *ad libitum*. All animal experiments were approved by the Institutional Animal Care and Use Committee of Hokkaido University and conducted in accordance with the institutional guidelines.

Skin Permeability Barrier Assay. TEWL was measured on the dorsal skin of E18.5 mice as described previously (21), using a Vapo Scan AS-VT100RS evaporimeter (Asch Japan, Tokyo, Japan). Toluidine blue staining was performed by incubating E18.5 mice with methanol for 5 min, washing with PBS, and then immersing in 0.1% (w/v) toluidine blue in PBS solution at 4 °C for 2 hr.

Histological Analyses. Hematoxylin/eosin staining and transmission electron microscopy on E18.5 mouse skin were performed as described previously (43).

Plasmids. A plasmid expressing 3×FLAG-tagged human *FATP4* gene (pCE-puro 3×FLAG-FATP4) was constructed by cloning the *FATP4* gene (39) into the *Bam*HI-*Not*I site of the mammalian expression vector pCE-puro 3×FLAG-1 (44).

***FATP4* Knockdown.** Lentiviral particles expressing an *FATP4* shRNA were prepared as previously described (27).

Lipid Analyses. LC-MS/MS analyses were performed as described previously (27). Separation of lipids by TLC using Silica gel 60 (Merck, Darmstadt, Germany) was conducted using two solvent systems. The solvent system for separation of ceramide and glucosylceramide species has been described previously (26); that for TAG, FA, and cholesterol species was hexane/diethyl ether/acetic acid (65:35:1, vol/vol). Lipids were detected by spraying a copper phosphoric acid solution [3% (wt/vol) $CuSO_4$ in 8% (vol/vol) aqueous phosphoric acid] onto TLC plates and heating at 180 °C for 10 min.

Statistical Analyses. Data are presented as means ± SD. The significance of differences between groups was evaluated using non-paired two-tailed Student's *t*-test or Dunnett's test in Microsoft Excel (Microsoft, Redmond, WA) or JMP13 (SAS Institute, Cary, NC), respectively. A *P*-value of < 0.05 was considered significant.

Data availability. All data generated in this study are included in this published article and its supplementary information.

Footnotes

H.Y. and M.H. performed the research and analyzed the data. W.C. provided materials. Y.O. performed the research, analyzed the data, and wrote the manuscript. A.K. planned the project, designed the experiments, and wrote the manuscript.

The authors declare no conflict of interest.

Acknowledgements

We thank Dr. Takayuki Sassa for technical support. This work was supported by funding from the Cosmetology Research Foundation (to A.K.), by the Advanced Research and Development Programs for Medical Innovation (AMED-CREST) Grant Number JP19gm0910002 (to A.K.) from Japan Agency for Medical Research and Development (AMED), and by KAKENHI Grant Numbers JP18H03976 (to A.K.), JP18H04664 (to A.K.), and JP15H05589 (to Y.O.) from the Japan Society for the Promotion of Science (JSPS).

References

1. V. Oji, et al., Revised nomenclature and classification of inherited ichthyoses: results of the First Ichthyosis Consensus Conference in Soreze 2009. *J. Am. Acad. Dermatol.* **63**, 607-641 (2010).
2. E. Goleva, E. Berdyshev, D. Y. Leung, Epithelial barrier repair and prevention of allergy. *J. Clin. Invest.* **129**, 1463-1474 (2019).
3. J. Klar, et al., Mutations in the fatty acid transport protein 4 gene cause the ichthyosis prematurity syndrome. *Am. J. Hum. Genet.* **85**, 248-253 (2009).
4. D. Khnykin, J. H. Miner, F. Jahnsen, Role of fatty acid transporters in epidermis: Implications for health and disease. *Dermatoendocrinol.* **3**, 53-61 (2011).
5. E. Bueno, et al., Novel mutations in FATP4 gene in two families with ichthyosis prematurity syndrome. *J. Eur. Acad. Dermatol. Venereol.* **31**, e11-e13 (2017).
6. A. Bygum, P. Westermark, F. Brandrup, Ichthyosis prematurity syndrome: a well-defined congenital ichthyosis subtype. *J. Am. Acad. Dermatol.* **59**, S71-74 (2008).
7. A. Kihara, Very long-chain fatty acids: elongation, physiology and related disorders. *J. Biochem.* **152**, 387-395 (2012).
8. A. Kihara, Synthesis and degradation pathways, functions, and pathology of ceramides and epidermal acylceramides. *Prog. Lipid Res.* **63**, 50-69 (2016).
9. T. Herrmann, et al., Mouse fatty acid transport protein 4 (FATP4): characterization of the gene and functional assessment as a very long chain acyl-CoA synthetase. *Gene* **270**, 31-40 (2001).
10. T. Herrmann, et al., Mice with targeted disruption of the fatty acid transport protein 4 (Fatp4, Slc27a4) gene show features of lethal restrictive dermopathy. *J. Cell Biol.* **161**, 1105-1115 (2003).

11. C. L. Moulson, et al., Cloning of wrinkle-free, a previously uncharacterized mouse mutation, reveals crucial roles for fatty acid transport protein 4 in skin and hair development. *Proc. Natl. Acad. Sci. U. S. A.* **100**, 5274-5279 (2003).

12. R. E. Gimeno, et al., Targeted deletion of fatty acid transport protein-4 results in early embryonic lethality. *J. Biol. Chem.* **278**, 49512-49516 (2003).

13. M. H. Lin, K. W. Chang, S. C. Lin, J. H. Miner, Epidermal hyperproliferation in mice lacking fatty acid transport protein 4 (FATP4) involves ectopic EGF receptor and STAT3 signaling. *Dev. Biol.* **344**, 707-719 (2010).

14. J. Tao, et al., A spontaneous *Fatp4*/*Scl27a4* splice site mutation in a new murine model for congenital ichthyosis. *PLoS One* **7**, e50634 (2012).

15. K. R. Feingold, P. M. Elias, Role of lipids in the formation and maintenance of the cutaneous permeability barrier. *Biochim. Biophys. Acta* **1841**, 280-294 (2014).

16. Y. Uchida, W. M. Holleran, Omega-*O*-acylceramide, a lipid essential for mammalian survival. *J. Dermatol. Sci.* **51**, 77-87 (2008).

17. T. Hirabayashi, M. Murakami, A. Kihara, The role of PNPLA1 in ω-*O*-acylceramide synthesis and skin barrier function. *Biochim. Biophys. Acta* **1864**, 869-879 (2019).

18. K. Sugiura, M. Akiyama, Update on autosomal recessive congenital ichthyosis: mRNA analysis using hair samples is a powerful tool for genetic diagnosis. *J. Dermatol. Sci.* **79**, 4-9 (2015).

19. V. Vasireddy, et al., Loss of functional ELOVL4 depletes very long-chain fatty acids (≥C28) and the unique ω-O-acylceramides in skin leading to neonatal death. *Hum. Mol. Genet.* **16**, 471-482 (2007).

20. R. Jennemann, et al., Loss of ceramide synthase 3 causes lethal skin barrier disruption. *Hum. Mol. Genet.* **21**, 586-608 (2012).

21. T. Sassa, et al., Impaired epidermal permeability barrier in mice lacking *Elovl1*, the gene responsible for very-long-chain fatty acid production. *Mol Cell Biol* **33**, 2787-2796 (2013).

22. S. Grond, et al., PNPLA1 deficiency in mice and humans leads to a defect in the synthesis of omega-O-acylceramides. *J. Invest. Dermatol.* **137**, 394-402 (2017).

23. T. Hirabayashi, et al., PNPLA1 has a crucial role in skin barrier function by directing acylceramide biosynthesis. *Nat. Commun.* **8**, 14609 (2017).

24. M. Pichery, et al., PNPLA1 defects in patients with autosomal recessive congenital ichthyosis and KO mice sustain PNPLA1 irreplaceable function in epidermal omega-O-acylceramide synthesis and skin permeability barrier. *Hum. Mol. Genet.* **26**, 1787-1800 (2017).

25. Y. Ohno, et al., ELOVL1 production of C24 acyl-CoAs is linked to C24 sphingolipid synthesis. *Proc. Natl. Acad. Sci. U. S. A.* **107**, 18439-18444 (2010).

26. Y. Ohno, et al., Essential role of the cytochrome P450 CYP4F22 in the production of acylceramide, the key lipid for skin permeability barrier formation. *Proc. Natl. Acad. Sci. U. S. A.* **112**, 7707-7712 (2015).

27. Y. Ohno, N. Kamiyama, S. Nakamichi, A. Kihara, PNPLA1 is a transacylase essential for the generation of the skin barrier lipid ω-*O*-acylceramide. *Nat. Commun.* **8**, 14610 (2017).

28. C. Lefèvre, et al., Mutations in a new cytochrome P450 gene in lamellar ichthyosis type 3. *Hum. Mol. Genet.* **15**, 767-776 (2006).

29. K. Sugiura, et al., Lamellar ichthyosis in a collodion baby caused by *CYP4F22* mutations in a non-consanguineous family outside the Mediterranean. *J. Dermatol. Sci.* **72**, 193-195 (2013).

30. A. Hotz, et al., Mutation update for *CYP4F22* variants associated with autosomal recessive congenital ichthyosis. *Hum. Mutat.* **39**, 1305-1313 (2018).

31. P. A. Watkins, D. Maiguel, Z. Jia, J. Pevsner, Evidence for 26 distinct acyl-coenzyme A synthetase genes in the human genome. *J. Lipid Res.* **48**, 2736-2750 (2007).

32. E. Candi, R. Schmidt, G. Melino, The cornified envelope: a model of cell death in the skin. *Nat. Rev. Mol. Cell Biol.* **6**, 328-340 (2005).

33. A. Muñoz-Garcia, C. P. Thomas, D. S. Keeney, Y. Zheng, A. R. Brash, The importance of the lipoxygenase-hepoxilin pathway in the mammalian epidermal barrier. *Biochim. Biophys. Acta* **1841**, 401-408 (2014).

34. P. M. Elias, et al., Formation and functions of the corneocyte lipid envelope (CLE). *Biochim. Biophys. Acta* **1841**, 314-318 (2014).

35. M. Miyamoto, N. Itoh, M. Sawai, T. Sassa, A. Kihara, Severe skin permeability barrier dysfunction in knockout mice deficient in a fatty acid ω-hydroxylase crucial to acylceramide production. *J. Invest. Dermatol.* in press.

36. Y. Ohno, A. Nara, S. Nakamichi, A. Kihara, Molecular mechanism of the ichthyosis pathology of Chanarin-Dorfman syndrome: Stimulation of PNPLA1-catalyzed ω-*O*-acylceramide production by ABHD5. *J. Dermatol. Sci.* **92**, 245-253 (2018).

37. M. Schmuth, et al., Differential expression of fatty acid transport proteins in epidermis and skin appendages. *J. Invest. Dermatol.* **125**, 1174-1181 (2005).

38. K. Nakahara, et al., The Sjögren-Larsson syndrome gene encodes a hexadecenal dehydrogenase of the sphingosine 1-phosphate degradation pathway. *Mol. Cell* **46**, 461-471 (2012).

39. A. Ohkuni, Y. Ohno, A. Kihara, Identification of acyl-CoA synthetases involved in the mammalian sphingosine 1-phosphate metabolic pathway. *Biochem. Biophys. Res. Commun.* **442**, 195-201 (2013).

40. T. Sassa, M. Tadaki, H. Kiyonari, A. Kihara, Very long-chain tear film lipids produced by fatty acid elongase ELOVL1 prevent dry eye disease in mice. *FASEB J.* **32**, 2966-2978 (2018).

41. Y. Honda, et al., Decreased skin barrier lipid acylceramide and differentiation-dependent gene expression in ichthyosis gene *Nipal4*-knockout mice. *J. Invest. Dermatol.* **138**, 741-749 (2018).

42. M. H. Lin, J. H. Miner, Fatty acid transport protein 1 can compensate for fatty acid transport protein 4 in the developing mouse epidermis. *J. Invest. Dermatol*. **135**, 462-470 (2015).

43. T. Naganuma, et al., Disruption of the Sjögren-Larsson syndrome gene *Aldh3a2* in mice increases keratinocyte growth and retards skin barrier recovery. *J. Biol. Chem.* **291**, 11676-11688 (2016).

44. A. Kihara, Y. Anada, Y. Igarashi, Mouse sphingosine kinase isoforms SPHK1a and SPHK1b differ in enzymatic traits including stability, localization, modification, and oligomerization. *J. Biol. Chem.* **281**, 4532-4539 (2006).

Figure legends

Fig. 1. Skin barrier dysfunction in *Fatp4* KO mice. (*A*) Structure of ceramide. (*B*) Structure of acylceramide and reactions that introduce ω-OH ULCFA into acylceramide. (*C*) Genome structure of mouse *Fatp4* gene and WT and mutant nucleotide sequences around CRISPR-Cas9 target sequence. The black boxes represent coding sequences. Red, inserted nucleotide in *Fatp4* KO mouse; blue, target sequence of the guide RNA; orange, protospacer adjacent motif (PAM) sequence. (*D*–*G*) WT and *Fatp4* KO mice were prepared by cesarean section at E18.5. (*D*) Photograph of specimens. Scale bar represents 1 cm. (*E*) Measurement of survival rates (WT, n = 4; KO, n = 3). (*F*) Measurement of body weights (WT, n = 4; KO, n = 4). (*G*) Measurement of TEWL (WT, n = 4; KO, n = 4). Values represent the means ± SDs. Statistically significant differences are indicated (two-tailed Student's *t*-test; **P*<0.05; ***P*<0.01). (*H*) WT and *Fatp4* KO mice at E18.5 were incubated with 0.1% toluidine blue solution for 2 h and photographed.

Fig. 2. Hyperkeratosis and impaired formation of lipid lamellae and keratohyalin granules in *Fatp4* KO mice. (*A*) Paraffin sections of E18.5 WT and *Fatp4* KO mouse skin were prepared and stained with hematoxylin and eosin, and bright field images were photographed. The scale bars represent 20 μm. (*B*–*D*) Ultrathin sections of E18.5 WT and *Fatp4* KO mouse skin were prepared and subjected to transmission electron microscopy. (*B*) Red arrowheads indicate keratohyalin granules. The scale bars represent 10 μm. (*C*) Enlarged views of the yellow boxes in (*B*). Magenta and light blue arrowheads indicate curved membrane structures and vacuoles in corneocytes, respectively. The scale bars represent 5 μm. (*D*) Enlarged views of the curved membrane structures observed in *Fatp4* KO mouse skin are shown. The scale bars represent 1 μm. SC, stratum corneum; SG, stratum granulosum; SS, stratum spinosum; SB, stratum basale.

Fig. 3. Decreased amounts of acylceramides in the epidermis of *Fatp4* KO mice. (*A*) Lipids were extracted from the epidermis of WT and *Fatp4* KO mice at postnatal day 0. Lipids (2.5 mg skin) were separated by TLC using the solvent system for separation of ceramide and glucosylceramide (left panel) and that for separation of TAG, FA, and cholesterol (right panel) and stained with copper phosphate. The asterisk represents unidentified lipid band. (*B*) Structures of saturated (left) and monounsaturated (right) acylceramides. The position of the double bond in the monounsaturated FA of acylceramide is n-9. Sphingosine is the most abundant long-chain base among mammalian long-chain bases. (*C–F*) Lipids were extracted from the epidermis of WT (n = 3) and *Fatp4* KO (n = 3) mice at postnatal day 0. LC-MS/MS analyses were performed on acylceramides (*C*), acyl-glucosylceramides (*D*), protein-bound ceramides (*E*), and ω-OH ceramides (*F*). The left panels show the amount of each lipid species, and the right panels show the total of saturated (S) species, total of monounsaturated (MU) species, and total of all species. (*G*) The metabolic pathway of ω-OH ULCFA, an intermediate of acylceramide. (*H*) Sum of the amounts of ω-OH acyl-CoA metabolites [acylceramide (*C*), acyl-glucosylceramide (*D*), protein-bound ceramide (*E*), and ω-OH ceramide (*F*)]. Values represent the means ± SDs. Statistically significant differences are indicated (two-tailed Student's *t*-test; **P*<0.05; ***P*<0.01). Chol, cholesterol; Acyl-Cer, acylceramide; Cer, ceramide; Acyl-GlcCer, acyl-glucosylceramide; GlcCer, glucosylceramides; GPL, glycerophospholipid.

Fig. 4. Effects of *Fatp4* disruption on ceramide, FA, and TAG levels. (*A–C*) Lipids were extracted from the epidermis of WT (n = 3) and *Fatp4* KO (n = 3) mice at postnatal day 0. LC-MS/MS analyses were performed on ceramides (*A*), FAs (*B*), and TAGs containing linoleic acid (*C*). (*A, B*) The graphs show the amount of each lipid species, and the insets show the total

of ≤C24 species, total of ≥C26 saturated (S) species, total of ≥C26 monounsaturated (MU) species, and total of all species. (*C*) The graph shows the amount of each TAG species containing linoleic acid (C18:2), while the inset shows the total TAG quantities. The numbers after "C18:2-" represent the sum of two FAs other than linoleic acid. For example, C32:1 indicates that the summed chain length and degree of unsaturation of the two FA chains are 32 and 1, respectively. Values represent the means ± SDs. Statistically significant differences are indicated (two-tailed Student's *t*-test; **P*<0.05; ***P*<0.01). n.d., not detected.

Fig. 5. Effects of *Fatp4* disruption on the expression levels of keratinocyte differentiation markers and acylceramide-synthesis related genes. Total RNA was prepared from the epidermis of WT (n = 3) and *Fatp4* KO (n = 3) mice at postnatal day 0. Real-time quantitative RT-PCR was performed on *Hprt1*, keratinocyte differentiation markers (*Krt14*, *Krt10*, *Flg*, and *Ivl*) (*A*), acylceramide-synthesis related gene (*Pnpla1*, *Cers3*, *Cyp4f39*, and *Abhd5*) (*B*), *Elovl* family members (*Elovl1-7*) (*C*), and *Fatp* family members (*Fatp1-6*) (*D*). Values represent the means ± SDs and indicate the relative amounts to *Hprt1*. Statistically significant differences are indicated (two-tailed Student's *t*-test; **P*<0.05; ***P*<0.01).

Fig. 6. ACS activity of FATP4 toward ω-OH ULCFA. HEK 293T cells were transfected with vector (pCE-puro 3×FLAG-1) or a plasmid encoding *3xFLAG-FATP4* (pCE-puro 3×FLAG-FATP4), and membrane fractions were prepared 24 h after transfection. Membrane fractions (20 μg) were incubated with 10 μM FA (ω-OH C30:0 FA, C24:0 FA, or C24:1 FA) and 0.5 mM CoA, 2.4 mM ATP at 37 °C for 1 h. The generated acyl-CoAs were extracted and quantified by LC-MS/MS. Values represent the means ± SDs obtained from three

independently prepared samples. Statistically significant differences are indicated (two-tailed Student's *t*-test; ***P*<0.01).

Fig. 7. Reduction in acylceramide levels with *FATP4* knockdown in human keratinocytes. Human keratinocytes were infected with lentiviral particles expressing control shRNA, sh*FATP4*-1, or sh*FATP4*-2, and then differentiation was induced for 7 days. (*A*) Total RNA was prepared, and real-time quantitative RT-PCR was performed for *GAPDH* and *FATP4*. Values represent the means ± SD obtained from three independent experiments and indicate the expression levels relative to *GAPDH*. (*B*–*C*) Lipids were extracted, and acylceramides (*B* and *C*) and (non-acylated) ceramides (*D*) were quantified by LC-MS/MS. The amount of each acylceramide species (*B*), total amount of acylceramides (*C*), and total amount of ceramides (*D*) are shown. Values represent the means ± SD obtained from three independent experiments. Statistically significant differences are indicated (Dunnett's test; **P* < 0.05; ***P* < 0.01). sh-1, sh*FATP4*-1; sh-2, sh*FATP4*-2.

Figure 1

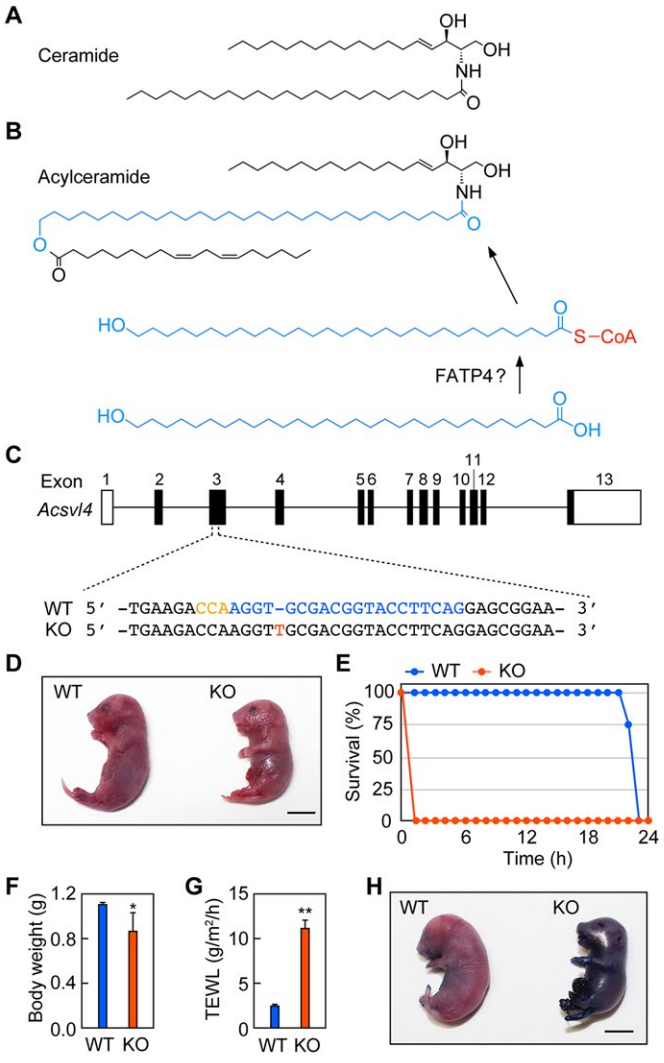
A
Ceramide
OH
OH
NH
O
B
Acylceramide
OH
OH
NH
O
O
O
HO
O
S−CoA
FATP4?
HO
O
OH
C
Exon 1 2 3 4 5 6 7 8 9 10 11 12 13
Acsvl4
WT 5′ -TGAAGACCAAGGT-GCGACGGTACCTTCAGGAGCGGAA- 3′
KO 5′ -TGAAGACCAAGGTTGCGACGGTACCTTCAGGAGCGGAA- 3′
D
WT
KO
E
WT
KO
Survival (%)
100
75
50
25
0
0
6
12
18
24
Time (h)
F
Body weight (g)
1.2
0.8
0.4
0.0
*
WT KO
G
TEWL (g/m²/h)
15
10
5
0
**
WT KO
H
WT
KO

Figure 2

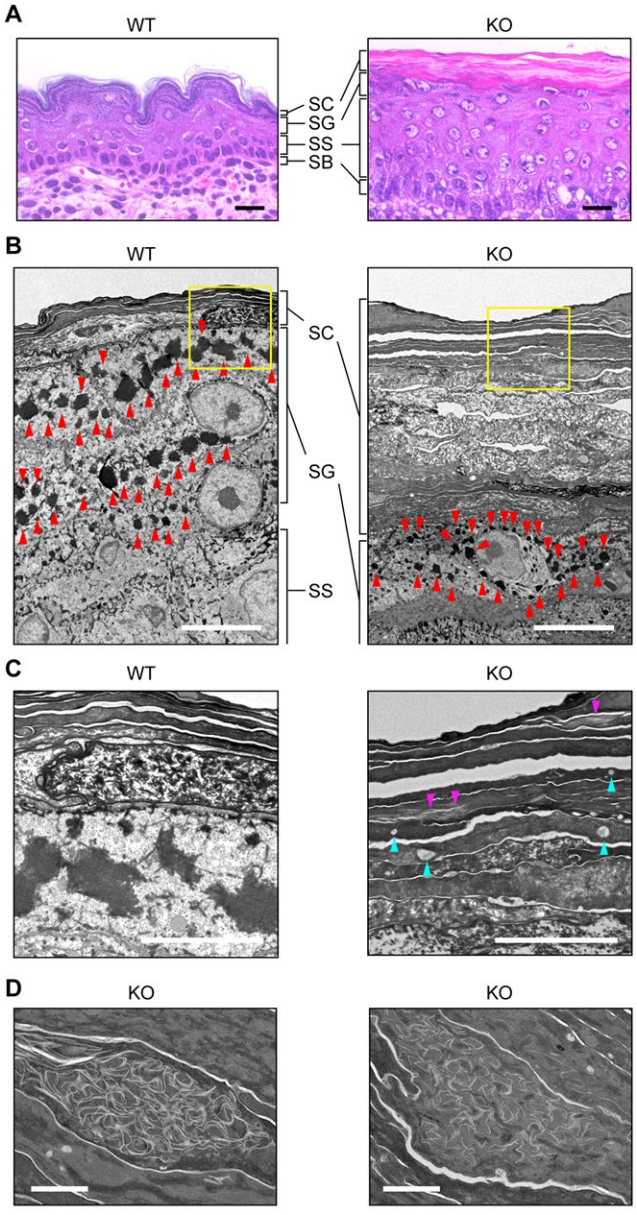

Figure 3

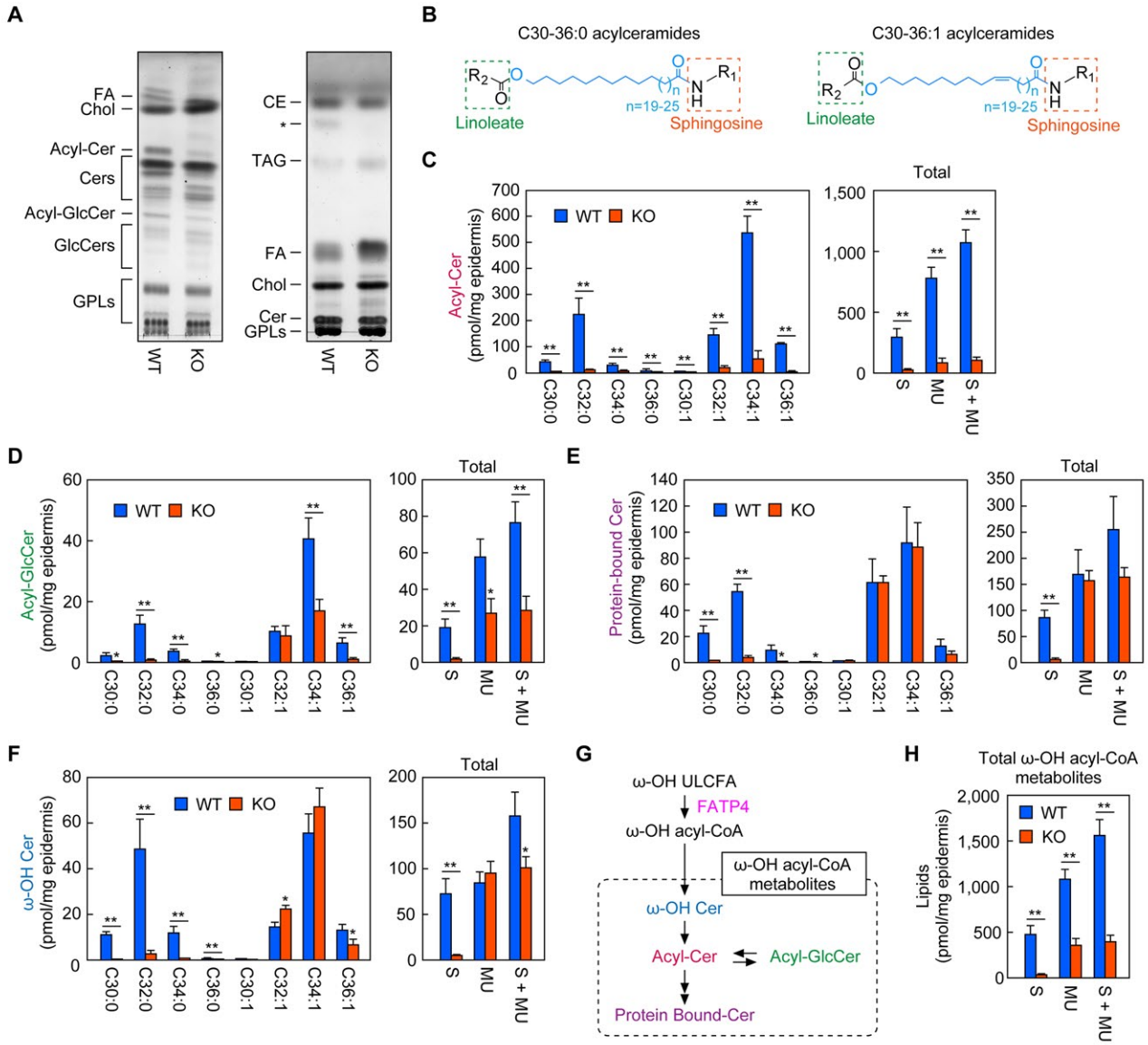
A
FA
Chol
Acyl-Cer
Cers
Acyl-GlcCer
GlcCers
GPLs
WT
KO
CE
*
TAG
FA
Chol
Cer
GPLs
B
C30-36:0 acylceramides
C30-36:1 acylceramides
Linoleate
n=19-25
Sphingosine
C
Acyl-Cer (pmol/mg epidermis)
WT
KO
C30:0
C32:0
C34:0
C36:0
C30:1
C32:1
C34:1
C36:1
Total
S
MU
S + MU
D
Acyl-GlcCer (pmol/mg epidermis)
E
Protein-bound Cer (pmol/mg epidermis)
F
ω-OH Cer (pmol/mg epidermis)
G
ω-OH ULCFA
FATP4
ω-OH acyl-CoA
ω-OH acyl-CoA metabolites
ω-OH Cer
Acyl-Cer
Acyl-GlcCer
Protein Bound-Cer
H
Total ω-OH acyl-CoA metabolites
Lipids (pmol/mg epidermis)

Figure 4

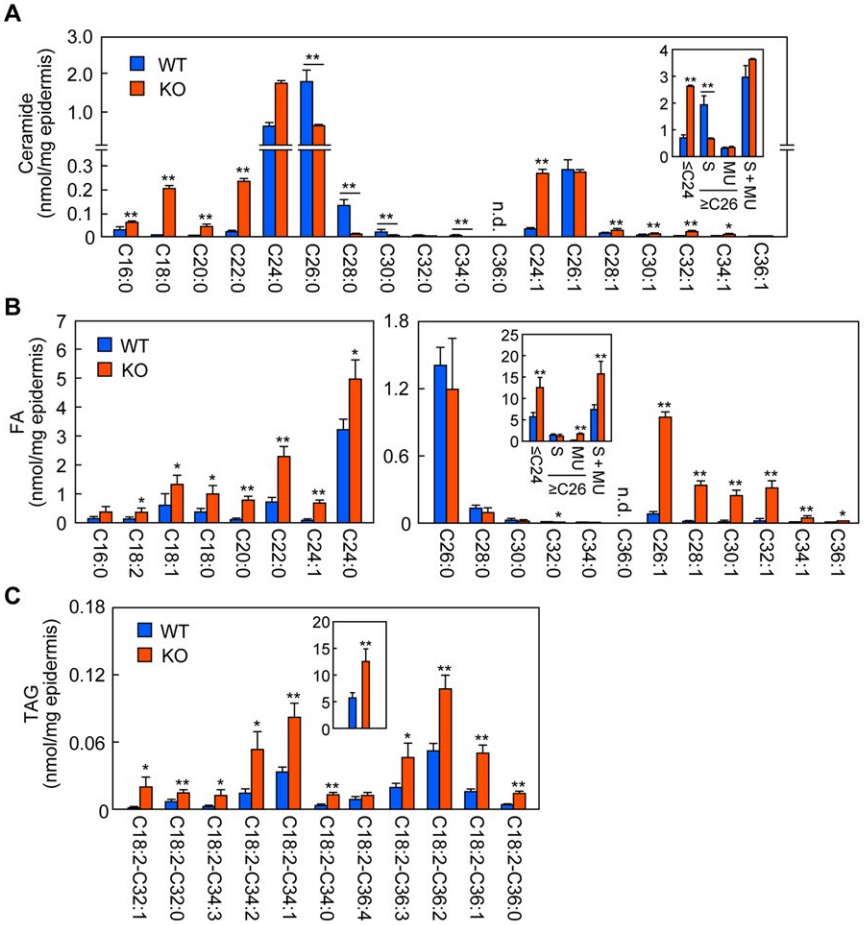
A
Ceramide (nmol/mg epidermis)
WT
KO
C16:0
C18:0
C20:0
C22:0
C24:0
C26:0
C28:0
C30:0
C32:0
C34:0
C36:0
C24:1
C26:1
C28:1
C30:1
C32:1
C34:1
C36:1
n.d.
≤C24
≥C26
S
MU
S+MU
B
FA (nmol/mg epidermis)
C16:0
C18:2
C18:1
C18:0
C20:0
C22:0
C24:1
C24:0
C26:0
C28:0
C30:0
C32:0
C34:0
C36:0
C26:1
C28:1
C30:1
C32:1
C34:1
C36:1
C
TAG (nmol/mg epidermis)
C18:2-C32:1
C18:2-C32:0
C18:2-C34:3
C18:2-C34:2
C18:2-C34:1
C18:2-C34:0
C18:2-C36:4
C18:2-C36:3
C18:2-C36:2
C18:2-C36:1
C18:2-C36:0

Figure 5

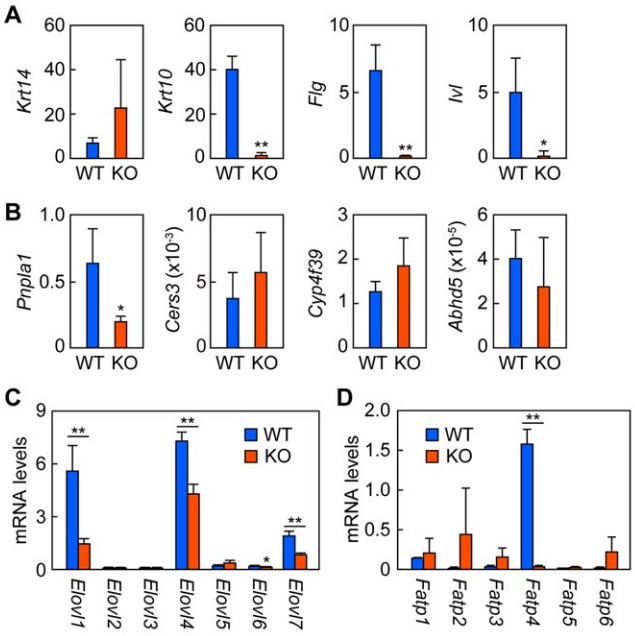
A
Krt14
Krt10
Flg
Ivl
WT KO
B
Pnpla1
Cers3 (x10-3)
Cyp4f39
Abhd5 (x10-5)
C
mRNA levels
WT
KO
Elovl1
Elovl2
Elovl3
Elovl4
Elovl5
Elovl6
Elovl7
D
Fatp1
Fatp2
Fatp3
Fatp4
Fatp5
Fatp6

Figure 6

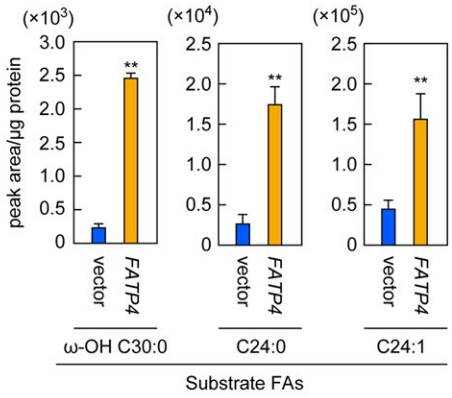
(×10^3)
(×10^4)
(×10^5)
peak area/μg protein
3.0
2.5
2.0
1.5
1.0
0.5
0
**
vector
FATP4
ω-OH C30:0
C24:0
C24:1
Substrate FAs

Figure 7

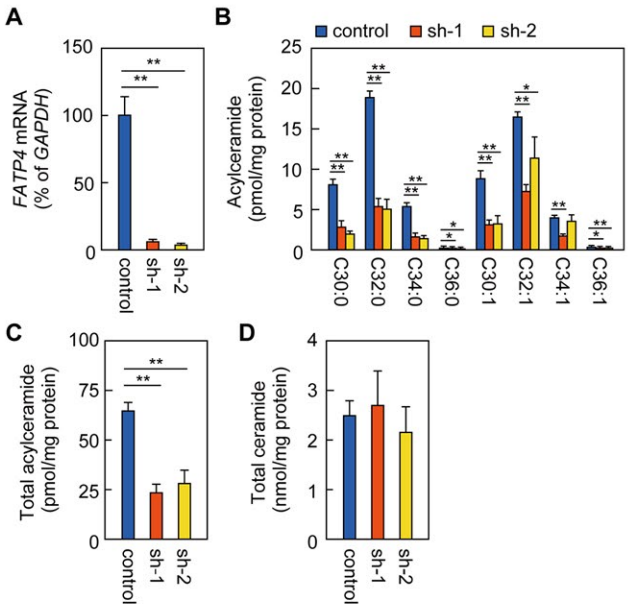
A
FATP4 mRNA (% of GAPDH)
150
100
50
0
control
sh-1
sh-2
B
control
sh-1
sh-2
Acylceramide (pmol/mg protein)
25
20
15
10
5
0
C30:0
C32:0
C34:0
C36:0
C30:1
C32:1
C34:1
C36:1
C
Total acylceramide (pmol/mg protein)
100
75
50
25
0
control
sh-1
sh-2
D
Total ceramide (nmol/mg protein)
4
3
2
1
0
control
sh-1
sh-2

SI Materials and Methods

Production and Breeding of Mice. C57BL/6J mice and *Fatp4* KO mice derived from them were used in this study. *Fatp4* KO mice were generated by CRISPR/Cas9 as follows. The two oligonucleotides 5'-CTGAAGGTACCGTCGCACCTGTTTT-3' and 5'-AGGTGCGACGGTACCTTCAGGGTG-3 were annealed to produce a guide RNA targeted to the exon 3 of *Fatp4* and cloned into the *Bbs*I site of the pX330 plasmid (Addgene, Watertown, MA). The resulting plasmid was injected into C57BL/6J mouse zygotes. Genome DNAs were prepared from the tails of the born mice and subjected to genotyping by PCR using primers 5'-CCCGGAAAAGGGAGCCTTGCC-3' and 5'-CAGACCCACAAACTCATTGCG-3' and DNA sequencing using the primer 5'-GGAGACTATGGGCTTGGGGC-3'. The *Fatp4* heterozygous KO mice were maintained by repeated back-crossing with C57BL/6J mice and were used for intercrosses to generate the *Fatp4* homozygous KO mice. Male and female mice were allowed to live together overnight for pregnancy, and the following noon was designated as E0.5. Newborn mice obtained by cesarean section at E18.5 or natural birth were used for analyses.

Histological Analyses. Hematoxylin/eosin staining was performed as described previously (1). Transmission electron microscopy was conducted as follows. Skin samples isolated from E18 mice were fixed with 4% paraformaldehyde and 2% glutaraldehyde in 0.1 M cacodylate buffer (pH 7.4) at 4 °C and additionally treated with 0.1% tannic acid in 0.1 M cacodylate buffer (pH 7.4) at 4 °C. Samples were then washed with 0.1 M cacodylate buffer (pH 7.4) four times and post-fixed with 2% osmium tetroxide in 0.1 M cacodylate buffer (pH 7.4) at 4 °C. After dehydration in graded ethanol solutions (50%, 70%, 90%, and 100%), samples were infiltrated with propylene oxide twice, for 1 h each, and were put into a propylene oxide/resin (Quetol-812; Nisshin EM, Tokyo, Japan) mixture (70:30) for 1 h. Propylene oxide was then volatilized by opening the cap of the tube. The samples were transferred to a fresh 100% resin and were polymerized at 60 °C for 48 h. Ultra-thin sections (70 or 80 nm) were prepared using an ultramicrotome (Ultracut UCT; Leica, Vienna, Austria) equipped with a diamond knife. The sections were mounted on copper grids, stained with 2% uranyl acetate at room temperature for 15 min, washed with water, and stained with a secondary lead stain solution (Merck, Darmstadt, Germany) at room temperature for 3 min. The grids were observed using a transmission electron microscope (JEM-1400Plus; JEOL, Tokyo, Japan) at an acceleration voltage of 100 kV. Images were taken using a charge-coupled device camera (EM-14830RUBY; JEOL).

Cell Culture. Human embryonic kidney (HEK 293T) and Lenti-X 293T (TAKARA Bio, Shiga, Japan) cells were cultured in Dulbecco's Modified Eagle's medium (D6429; Merck) containing 10% FBS (Thermo Fisher Scientific, Waltham, MA), 100 units/mL penicillin, and 100 μg/mL streptomycin (Merck) on collagen-coated dishes. Primary human keratinocytes (CELLnTEC, Bern, Switzerland) were cultured in CnT-prime epithelial culture medium (CELLnTEC). Cells were grown at 37 °C under 5% CO_2.

***FATP4* Knockdown.** Lentiviral particles expressing a *FATP4* shRNA were essentially prepared as described previously (2). Two pairs of DNA oligos targeting FATP4 (sh*FATP4*-1-F and -R or sh*FATP4*-2-F and -R; *SI Appendix*, Table S1) were annealed and cloned into the shRNA vector pAK1072, which contains the U6 promoter, generating the pYU574 and pYU655 plasmid, respectively. The U6-shRNA region of the pYU574 or pYU655 plasmid was then transferred to the lentiviral vector pNS64, producing the pYU577 or pYU657 plasmid, respectively. Lenti-X 293T cells were transfected with the pYU577 or pYU657 plasmid, together with the lentiviral packaging plasmid psPAX2 and the VSV-G envelope-expressing plasmid pMD2.G (both from Addgene, Cambridge, MA). The medium was changed to fresh Dulbecco's Modified Eagle's medium containing 10% FBS at 24 and 48 h after transfection. The media collected at 48 and 72 h after transfection were pooled and centrifuged (50,000 × g, 4 °C, 2 h) to concentrate the lentiviral particles. The concentrated lentiviral particles were then used to infect human keratinocytes at 37 °C for 6 h. The medium was changed to fresh media without lentiviral particles, and cells were cultured for 3 days. Differentiation was then induced by incubating the infected cells in CnT-Prime 3D Barrier medium (CELLnTEC) for 7 days.

Lipid Analyses. After incubating with PBS at 55 °C for 5 min, mouse skin was separated into epidermis and dermis. The obtained epidermis (wet weight 10 mg) was transferred to tubes containing zirconia beads and treated with 450 μL $CHCl_3$/MeOH (1:2, vol/vol) and internal standard mix [500 pmol N-palmitoyl (d_9) D-*erythro*-sphingosine (Avanti Polar Lipids, Alabaster, AL), 500 pmol d_{31}-palmitic acid (Cayman Chemical, Ann Arbor, MI), and Mouse SPLASH LIPIDOMIX Mass Spec Internal Standard containing 10 pmol C15:0- d_7-C18:1-C15:0 TAG (Avanti Polar Lipids)]. Lipids were extracted by vigorous mixing (4,500 rpm) at 4 °C for 1 min using the Micro Homogenizing System Micro Smash MS-100 (Tomy Seiko, Tokyo, Japan). Samples were then centrifuged (20,400 × g, room temperature, 3 min), and the supernatant was recovered. The pellet was again treated with 450 μL $CHCl_3$/MeOH (1:2, vol/vol), vigorously mixed, and centrifuged, and the resulting supernatant was combined with the first supernatant. The remaining pellet was used for extraction of protein-bound ceramides (see below). The pooled supernatant was treated with 300 μL of $CHCl_3$ and 540 μL H_2O, vigorously mixed, and centrifuged (20,400 × g, room temperature, 3 min). The organic phase containing lipids was recovered and dried. The lipids were dissolved in 100 μL $CHCl_3$/MeOH (1:2, vol/vol). After diluting the lipids 100 times, 5 μL (corresponding to 5 μg of epidermis) was subjected to LC-MS/MS analyses for quantification of acylceramides, acyl-glucosylceramides, ω-OH ceramides, ceramides, and TAGs as described below. Alternatively, for quantification of FAs, 2 μL of lipid extracts were dried and derivatized to *N*-(4-aminomethylphenyl)pyridinium (AMPP) amides using the AMP+ Mass Spectrometry Kit (Cayman Chemical), according to the manufacturer's manual. Samples were then diluted 10 times, and 2 μL (corresponding to 2 μg of epidermis) was subjected to LC-MS/MS as described below.

Extraction of protein-bound ceramides was performed as follows. The pellet obtained during the above lipid extraction procedure was washed 3 times with 1 mL of MeOH and incubated with 1 mL of 95% MeOH at 60 °C for 2 h. After centrifugation (20,400 × g, room temperature, 3 min), the supernatant was removed. The pellet was again incubated with 1 mL 95% MeOH at 60 °C for 2 h and centrifuged (20,400 × g, room temperature, 3 min). After removal of the supernatant, the resulting pellet was incubated with 1 mL 1 M KOH in 95% MeOH at 60 °C for 2 h to release protein-bound ceramide. Then, 1 mL of 1 M acetic acid was added to the samples for neutralization, followed by addition of 1 mL of $CHCl_3$, mixing, and centrifugation (20,400 × g, room temperature, 3 min). The organic phase was recovered and dried. Lipids were dissolved in 100 μL of $CHCl_3$/MeOH (1:2, vol/vol), diluted 100 times, and 5 μL (corresponding to 5 μg of epidermis) was subjected to LC-MS/MS analyses.

LC-MS/MS analyses were performed as described previously (2). Lipids were separated by ultra-performance LC (UPLC) on a reverse-phase column (Acquity UPLC CSH C18 column; particle size, 1.7 μm; inner diameter, 2.1 mm; length, 100 mm; Waters, Milford, MA) and detected by electrospray ionization (ESI)–triple quadrupole spectrometer (Xevo TQ-S; Waters) in positive ion mode. Multiple reaction monitoring (MRM) measurement was performed using the *m/z* values for detection of precursor ions and product ions at quadrupole mass filters Q1 and Q3, respectively, and collision energies (*SI Appendix*, Tables S2–6). Data were analyzed using MassLynx software (Waters), and quantification was performed by calculating from the ratios to the internal standards.

***In Vitro* ACS Assay.** HEK 293T cells were transfected with pCE-puro 3xFLAG-1 (vector) or pCE-puro 3xFLAG-FATP4 plasmid using Lipofectamine Reagent and Plus Reagent (Thermo Fisher Scientific). After 24 h, the cells were washed with PBS and suspended in 300 μL lysis buffer [50 mM HEPES-NaOH (pH 7.5), 150 mM NaCl, 10% glycerol, 1 × protease inhibitor cocktail (Complete, EDTA-free protease inhibitor Cocktail; Merck), 1 mM phenylmethylsulfonyl fluoride, and 1 mM dithiothreitol]. Cells were lysed by sonication, and cell debris was removed by centrifugation (1,000 × g, 4 °C, 3 min). The supernatant was recovered and subjected to ultracentrifugation (100,000 × g, 4 °C, 35 min). The resulting pellet (membrane fraction) was suspended in 100 μL reaction buffer [lysis buffer containing 2.4 mM ATP, 8 mM $MgCl_2$, 20 mM NaF, 0.1% n-octyl-β-D-glucopyranoside, and 2 mM EDTA]. The enzyme reaction was carried out by incubating the membrane fractions (20 μg) with 10 μM FA [lignoceric acid (C24:0 FA; Merck), nervonic acid (C24:1 FA; Merck), or 30-hydroxytriacontanoic acid (ω-OH C30:0 FA, Nagara

Science, Gifu, Japan)], and 0.5 mM CoA at 37 °C for 1 h. After the reaction, 100 μL of water-saturated 1-butanol was added to extract the reaction products acyl-CoAs, mixed vigorously, and centrifuged (20, 400 × g, room temperature, 5 min). The extraction steps were repeated twice, and the organic phases were pooled, dried, and dissolved in 50 μL of 2-propanol/H_2O (1:1, vol/vol), of which 5 μL was subjected to LC-MS/MS analyses to quantify acyl-CoA levels. Lipids were separated by UPLC on a reverse-phase column (Acquity BEH C8 column; particle size, 1.7 μm; inner diameter, 2.1 mm; length 150 mm; Waters) with the column temperature at 40 °C. The flow rate was 0.15 mL/min in a binary gradient system using a mobile phase A [2-propanol/H_2O (85:15, vol/vol), adjusted to pH 11 with ammonia] and a mobile phase B (2-propanol, adjusted to pH 11 with ammonia). The elution gradient was set as follows: 0 min, 100% A; 0–6 min, gradient to 20% B; 6–24 min, gradient to 50% B; 24–24.1 min, gradient to 100% B; 24.1–26 min, 100% B; 26–26.1 min, gradient to 100% A; 26.1–30 min 100% A. The reaction products, acyl-CoAs, were detected by MRM using the ESI–triple quadrupole mass spectrometer Xevo TQ-S in positive ion mode. The *m/z* values of the precursor ions and fragment ions were set to detect at the Q1 and Q3 filters, respectively (*SI Appendix*, Table S7). Data were analyzed using MassLynx software (Waters).

Quantitative RT-PCR. After incubating with PBS at 55 °C for 5 min, mouse skin was separated into epidermis and dermis. Total RNA was prepared from epidermis (5 mg) using NucleoSpin RNA II Kit (Takara Bio), followed by conversion to cDNA using PrimeScript II 1st Strand cDNA Synthesis Kit (Takara Bio) and oligo dT primer. Real-time quantitative PCR was performed using the KOD SYBR qPCR Mix (Toyobo, Osaka, Japan) and forward (-F) and reverse (-R) primers for respective genes (*SI Appendix*, Table S1) on a CFX96 Touch Real-Time PCR Detection System (Bio-Rad, Hercules, CA).

Immunoblotting. Immunoblotting was performed as previously described (3) using anti-filaggrin rabbit polyclonal antibody (1/2,000 dilution; Covance, Trenton, NJ), anti-keratin 10 rabbit polyclonal antibody (1/500 dilution; BioLegend, San Diego, CA), or anti-GAPDH mouse monoclonal antibody 5A12 (1/2,000 dilution; FUJIFILM Wako Pure Chemical Corporation, Osaka, Japan) as a primary antibody. Anti-rabbit or anti-mouse IgG HRP-Linked $F(ab')_2$ fragment (1/7,500 dilution; GE Healthcare Life Sciences, Little Chalfont, UK) was used as a secondary antibody.

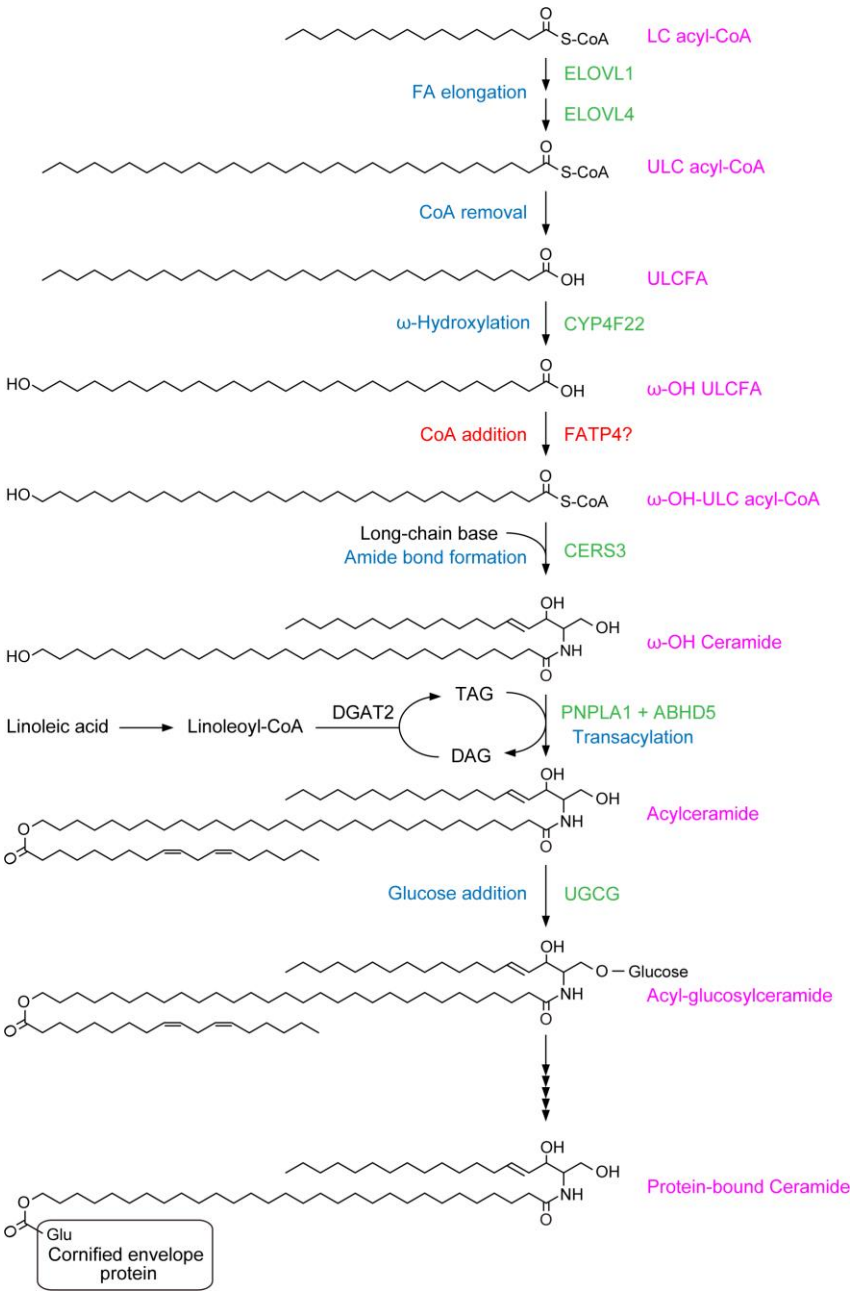

Fig. S1. Acylceramide synthesis pathway. LC acyl-CoAs is elongated to ULC acyl-CoA on the endoplasmic reticulum membrane by the FA elongases ELOVL1 and ELOVL4. After removal of CoA, ULCFA is ω-hydroxylated by CYP4F22, producing ω-OH ULCFA. ω-OH ULCFA is then re-converted to the acyl-CoA form by an unidentified ACS, and the resulting ω-OH ULC acyl-CoA is condensed with a long-chain base by the ceramide synthase CERS3 to generate ω-OH ceramide. The transacylase PNPLA1 transfers linoleic acid in TAG to ω-OH ceramide, creating acylceramide. ABHD5 enhances the utilization of TAG by PNPLA1. Acylceramide is produced from the upper part of the stratum spinosum throughout the stratum granulosum. After synthesis, acylceramide is rapidly converted to acyl-glucosylceramide by the addition of a glucose molecule, and is then stored in granules called lamellar bodies. Acyl-glucosylceramide is released to extracellular spaces at the interface of the stratum granulosum and stratum corneum and re-

converted to acylceramide by removal of the glucose residue. Most of the generated acylceramide is incorporated into lipid lamellae, while some is further converted to protein-bound ceramide on the surface of corneocytes via several steps: peroxidation, epoxidation, and epoxide hydrolysis on the linoleic acid moiety, followed by hydrolysis of the oxygenated linoleate moiety and covalent bonding of the exposed ω-OH group to the cornified envelope proteins. We hypothesized that FATP4 is responsible for the step of CoA addition to ω-OH ULCFA and examined this hypothesis in this study.

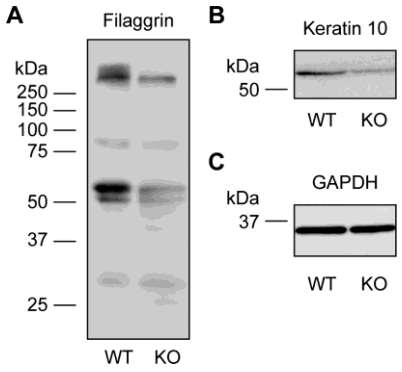

Fig. S2. The levels of filaggrin and keratin 10 proteins are decreased in *Fatp4* KO mice. Total cell lysates were prepared from E18.5 WT and *Fatp4* KO mouse epidermis samples and subjected to immunoblotting with anti-filaggrin (*A*), anti-keratin10 (*B*), or anti-GAPDH antibody (*C*; loading control).

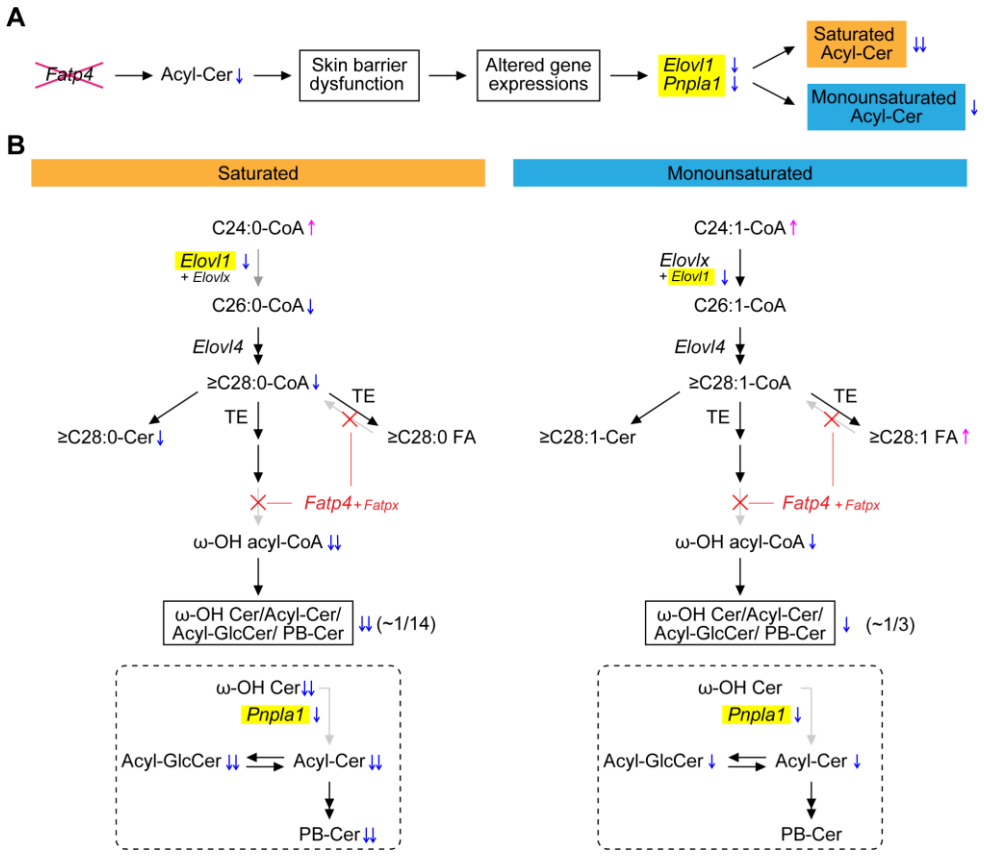

Fig. S3. Working model of the effects of *Fatp4* disruption on lipid metabolism. (A) *Fatp4* disruption causes skin barrier dysfunction through a decrease in acylceramide synthesis, which in turn affects expressions of various genes including *Elovl1* and *Pnpla1*. The reductions in *Elovl1* and *Pnpl1* expression further reduce acylceramide production, which effect is particularly prominent on saturated acylceramide. (B) Since the contribution of *Elovl1* to the elongation of saturated VLC acyl-CoAs is high, the lowered expression of *Elovl1* decreases the amount of Fatp4 substrate ω-OH ULCFA. Therefore, the large decreases in saturated acylceramide as well as whole ω-OH ULC acyl-CoA metabolites (ω-OH ceramide, acylceramide, acyl-glucosylceramide, protein-bound ceramide; dotted box) are caused both by direct effect of *Fatp4* disruption – the reduced reaction of ω-OH ULCFAs to ω-OH ULC acyl-CoAs in the acylceramide synthetic pathway – and by indirect effect of *Elovl1* decrease. On the other hand, since the contribution of *Elovl1* to the elongation of the monounsaturated VLC acyl-CoAs is low, the reduced *Elovl1* expression has almost no effect on syntheses of acylceramide and other ω-OH ULC acyl-CoA metabolites. Therefore, the decreases in monounsaturated acylceramide and whole ω-OH ULC acyl-CoA metabolites can only be attributed to the direct effect of *Fatp4* disruption. Since *Fatp4* deficiency also causes a decrease in *Pnpla1* expression, conversion of ω-OH ceramide to acylceramide is reduced. Some of the VLC/ULC acyl-CoAs produced by Elovl1 and Elovl4 are converted to VLCFAs/ULCFAs by thioesterases. Fatp4 functions not only in converting ω-OH ULCFAs to ω-OH ULC-CoAs in the acylceramide synthetic pathway, but also in converting these VLCFAs/ULCFAs back to VLC/ULC acyl-CoAs. Therefore, *Fatp4* deficiency creates a situation where VLCFAs/ULCFAs tend to accumulate. *Elovlx* and *Fatpx* represent *Elovl* family members other than *Elovl1* and *Fatp* subfamily members other than *Fatp4*, respectively, with text sizes indicating the degree of the contribution to the indicated reactions. *Elovlx* and *Fatpx* have overlapping functions with *Elovl1* and *Fatp4* in the acylceramide synthetic pathway,

respectively. Acyl-Cer, acylceramide; Cer, ceramide; Acyl-GlcCer, acyl-glucosylceramide; PB-Cer, protein-bound ceramide; TE, thioesterase; red arrow, increase; and blue arrow, decrease.

Table S1. DNA oligos and primers used in this study.

Oligo DNA/primer	Sequence
sh*FATP4*-1-F	5'-ACCTCGACCCGCTGTTCTATCTAGTTCAAGAGACTAGATAGAACAGCGGGTCTT-3'
sh*FATP4*-1-R	5'-CAAAAAGACCCGCTGTTCTATCTAGTCTCTTGAACTAGATAGAACAGCGGGTCG-3'
sh*FATP4*-2-F	5'-ACCTCGGTGAAGGCAAAGGTGCGATTCAAGAGATCGCACCTTTGCCTTCACCTT-3'
sh*FATP4*-2-R	5'-CAAAAAGGTGAAGGCAAAGGTGCGATCTCTTGAATCGCACCTTTGCCTTCACCG-3'
hFATP4-F	5'-AATGGCCTCAGCCATCTGTGAG-3'
hFATP4-R	5'-AGAGGGTCCAGGTGTTCTGTGC-3'
hGAPDH-F	5'-GAACGGGAAGCTCACTGGCATGGCC-3'
hGAPDH-R	5'-TGTCATACCAGGAAATGAGCTTGAC-3'
mKrt14-F	5'-CAACAGCGAGCTGGTGCAGAGCGGC-3'
mKrt14-R	5'-TAGGTGGCGATCTCCTGCTCCAGCC-3'
mKrt10-F	5'-GTGTCCACTGGTGATGTGAATGTGG-3'
mKrt10-R	5'-TTCTGTTTCTGCCAAGGAGGCTTCC-3'
mFlg-F	5'-CAACAATACTCAACCAGTGATAAGG-3'
mFlg-R	5'-CAGTTTTACTTCTCCCATTTGATCC-3'
mIvl-F	5'-ACACACTGCCAGTGACTGTTCCAGC-3'
mIvl-R	5'-CTTCTCCAGATGCAGTTCCTGTTCC-3'
mPnpla1-F	5'-CCCCACAAGCCTCTGCTGGTGGAGG-3'
mPnpla1-R	5'-TGGCCACTCACTCCCTCGGGGTAGC-3'
mAbhd5-F	5'-ATCACACCTTAAAGAAGCTGAAGAG-3'
mAbhd5-R	5'-AATGGATTCCACAAACTGATTCTCC-3'
mCers3-F	5'-CTGGCTTCCTCCAACAATAAAGTGG-3'
mCers3-R	5'-TCAAGTTACACTTCTTTGCCAGTCC-3'
mCyp4f39-F	5'-AGCATCTACGGGACCCACCACAACC-3'
mCyp4f39-R	5'-TGAGGGTAGAGGCTCTACATTGAGC-3'
mElovl1-F	5'-CATGCTTTCCAAGGTCATTGAGCTG-3'

mElovl1-R	5'-TCTCAGTTGGCCTTGACCTTGGTGG-3'
mElovl2-F	5'-GTTCCTGGACACGATTTTCTTTGTTC-3'
mElovl2-R	5'-TTATTGAGCCTTCTTGTCCGTCC-3'
mElovl3-F	5'-GCTTTGCCATCTACACGGATGACGC-3'
mElovl3-R	5'-TCATTGGCTCTTGGATGCAACTTTGC-3'
mElovl4-F	5'-GAGGAAGAAAAACAACCAAGTCTCC-3'
mElovl4-R	5'-AATTTACTCTCCTTTTGGCTTCCCG-3'
mElovl5-F	5'-AAGAACAACCACCAGATCACCGTGC-3'
mElovl5-R	5'-TCAATCCTTTCGCTGCTTCCTGGGC-3'
mElovl6-F	5'-GAGTTTTTACAATGGACCTGTCAGC-3'
mElovl6-R	5'-CTACTCAGCCTTCGTGGCTTTCTTC-3'
mElovl7-F	5'-CTGGCTTTATTACTTCTCCAAATTC-3'
mElovl7-R	5'-GTATTTTAGTGGCGCTTGCTTTTGC-3'
mFatp1-F	5'-CCCTCTTCGGGTGCTTCTC-3'
mFatp1-R	5'-TCCATTTTCCTACTCTCACAGGTG-3'
mFatp2-F	5'-CCTGGTGGTTTAGCTCATGACA-3'
mFatp2-R	5'-TTAAAGTTGGATTCTACGTATGAAGTGG-3'
mFatp3-F	5'-CAGCTCTACAGCCATGTTTCTGA-3'
mFatp3-R	5'-CAAAGATTCCTGGAGCCTGAGA-3'
mFatp4-F	5'-GCCCTGGACCCAGGTGGGATTCTCC-3'
mFatp4-R	5'-GAGTACTCATCCAGCTGGCGGAAGG-3'
mFatp5-F	5'-GGACCACTGGACTCCCAAAG-3'
mFatp5-R	5'-GACAGCACGTTGCTCACTTG-3'
mFatp6-F	5'-GGCTTGAGGATGCCGCTTA-3'
mFatp6-R	5'-GTACTCTGGGCTCATGCTATGAAGT-3'

h, human; m, mouse.

Table S2. Selected *m/z* values and collision energies for acylceramide species in MS/MS analysis.

Acylceramide species	Precursor ions (Q1)		Product ion (Q3)	Collision energy (eV)
	$[M–H_2O + H]^+$	$[M + H]^+$		
d18:1/C30:1/C18:2	992.8	1010.8	264.3	40
d18:1/C30:0/C18:2	994.8	1012.8	264.3	40
d18:1/C32:1/C18:2	1020.8	1038.8	264.3	40
d18:1/C32:0/C18:2	1022.8	1040.8	264.3	40
d18:1/C34:1/C18:2	1048.8	1066.8	264.3	40
d18:1/C34:0/C18:2	1050.8	1068.8	264.3	40
d18:1/C36:1/C18:2	1076.8	1094.8	264.3	40
d18:1/C36:0/C18:2	1078.8	1096.8	264.3	40

Table S3. Selected *m/z* values and collision energies for acyl-glucosylceramide species in LC-MS/MS analysis.

Acyl-glucosylceramide species	Precursor ions (Q1)		Product ion (Q3)	Collision energy (eV)
	$[M–H_2O + H]^+$	$[M + H]^+$		
d18:1/C30:1/C18:2	1154.9	1172.9	264.3	40
d18:1/C30:0/C18:2	1156.9	1174.9	264.3	40
d18:1/C32:1/C18:2	1182.9	1200.9	264.3	40
d18:1/C32:0/C18:2	1184.9	1202.9	264.3	40
d18:1/C34:1/C18:2	1210.9	1228.9	264.3	40
d18:1/C34:0/C18:2	1212.9	1230.9	264.3	40
d18:1/C36:1/C18:2	1238.9	1256.9	264.3	40
d18:1/C36:0/C18:2	1240.9	1258.9	264.3	40

Table S4. Selected *m/z* values and collision energies for ceramide species in LC-MS/MS analysis.

Ceramide species	Precursor ion (Q1)		Product ion (Q3)	Collision energy (eV)
	$[M–H_2O + H]^+$	$[M + H]^+$		
d18:1/C16:0	520.5	538.5	264.3	20
d18:1/C18:0	548.6	566.6	264.3	20
d18:1/C20:0	576.6	594.6	264.3	25
d18:1/C22:0	604.6	622.6	264.3	25
d18:1/C24:1	630.6	648.6	264.3	30
d18:1/C24:0	632.6	650.6	264.3	30
d18:1/C26:1	658.7	676.7	264.3	30
d18:1/C26:0	660.7	678.7	264.3	30
d18:1/C28:1	686.7	704.7	264.3	30
d18:1/C28:0	688.7	706.7	264.3	30
d18:1/C30:1	714.7	732.7	264.3	35
d18:1/C30:0	716.7	734.7	264.3	35
d18:1/C32:1	742.8	760.8	264.3	35
d18:1/C32:0	744.8	762.8	264.3	35
d18:1/C34:1	770.8	788.8	264.3	40
d18:1/C34:0	772.8	790.8	264.3	40
d18:1/C36:1	798.8	816.8	264.3	40
d18:1/C36:0	800.8	818.8	264.3	40
d18:1/ω-OH C30:1	730.7	748.7	264.3	35
d18:1/ω-OH C30:0	732.7	750.7	264.3	35
d18:1/ω-OH C32:1	758.7	776.7	264.3	35
d18:1/ω-OH C32:0	760.7	778.7	264.3	35
d18:1/ω-OH C34:1	786.7	804.7	264.3	40
d18:1/ω-OH C34:0	788.7	806.7	264.3	40

d18:1/ω-OH C36:1	814.7	832.7	264.3	40
d18:1/ω-OH C36:0	816.7	834.7	264.3	40
d18:1/d_9-C16:0[a]	529.5	547.5	264.3	20

[a]Internal standard.

Table S5. Selected *m/z* values and collision energies for TAG species in LC-MS/MS analysis.

TAG species	Precursor ion (Q1) $[M + NH_4]^+$	Product ion (Q3)	Collision energy (eV)
C18:2-C32:1	846.7	549.5	20
C18:2-C32:0	848.7	551.5	20
C18:2-C34:3	870.7	573.5	20
C18:2-C34:2	872.7	575.5	20
C18:2-C34:1	874.7	577.5	20
C18:2-C34:0	876.7	579.5	20
C18:2-C36:4	896.7	599.5	20
C18:2-C36:3	898.7	601.5	20
C18:2-C36:2	900.7	603.5	20
C18:2-C36:1	902.7	605.5	20
C18:2-C36:0	904.7	607.5	20
C18:1-C34:0	878.7	579.5	20
C18:1-C36:1	904.7	605.5	20
C18:1-C36:0	906.7	607.5	20
C15:0-d_7-C18:1-C15:0[a]	829.7	523.5	20

[a]Internal standard.

Table S6. Selected *m/z* values and collision energies for FA species in LC-MS/MS analysis.

FA species	Precursor ion (Q1) $[M + H]^+$	Product ion (Q3)	Collision energy (eV)
C16:1	421.6	239.0	48
C16:0	423.6	239.0	50
C18:2	447.6	239.0	44
C18:1	449.6	239.0	48
C18:0	451.6	239.0	50
C20:1	477.6	239.0	48
C20:0	479.6	239.0	50
C22:1	505.6	239.0	48
C22:0	507.6	239.0	50
C24:1	533.7	239.0	48
C24:0	535.7	239.0	50
C26:1	561.7	239.0	48
C26:0	563.7	239.0	50
C28:1	589.7	239.0	48
C28:0	591.7	239.0	50
C30:1	617.7	239.0	48
C30:0	619.7	239.0	50
C32:1	645.8	239.0	48
C32:0	647.8	239.0	50
C34:1	673.8	239.0	48
C34:0	675.8	239.0	50
C36:1	701.8	239.0	48
C36:0	703.8	239.0	50
ω-OH C30:1	633.6	239.0	48
ω-OH C30:0	635.6	239.0	50

ω-OH C32:1	661.6	239.0	48
ω-OH C32:0	663.6	239.0	50
ω-OH C34:1	689.6	239.0	48
ω-OH C34:0	691.7	239.0	50
ω-OH C36:1	717.7	239.0	48
ω-OH C36:0	719.7	239.0	50
d_{31}-C16:0[a]	454.6	242.0	50

[a]Internal standard.

Table S7. Selected *m/z* values and collision energies for acyl-CoA species in LC-MS/MS analysis.

Acyl-CoA species	Precursor ion (Q1) $[M + H]^+$	Product ion (Q3)	Collision energy (eV)
C24:0-CoA	1118.6	611.6	30
C24:1-CoA	1116.6	609.6	30
ω-OH C30:0-CoA	1218.6	711.6	30

SI References

1. T. Naganuma, et al., Disruption of the Sjögren-Larsson syndrome gene *Aldh3a2* in mice increases keratinocyte growth and retards skin barrier recovery. *J. Biol. Chem.* 291, 11676-11688 (2016).
2. Y. Ohno, N. Kamiyama, S. Nakamichi, A. Kihara, PNPLA1 is a transacylase essential for the generation of the skin barrier lipid ω-*O*-acylceramide. *Nat. Commun.* 8, 14610 (2017).
3. T. Kitamura, S. Takagi, T. Naganuma, A. Kihara, Mouse aldehyde dehydrogenase ALDH3B2 is localized to lipid droplets via two C-terminal tryptophan residues and lipid modification. *Biochem. J.* 465, 79-87 (2015).